FACULDADE DE ENGENHARIA DA UNIVERSIDADE DO PORTO

Combined heat and power production based on the supercritical water gasification of brewery residues

Augusto Miguel Fernandes Barbosa

Mestrado em Engenharia Mecânica

Supervisor: Prof.Eliseu Monteiro

October 9, 2023

Combined heat and power production based on the supercritical water gasification of brewery residues

Augusto Miguel Fernandes Barbosa

Mestrado em Engenharia Mecânica

October 9, 2023

Abstract

Biomass is widely used as a energy source for power production due to high calorific powers, worldwide availability and a neutral carbon footprint.

Huge amounts of brewery's spent grains (BSG) are obtained from beer production across the world and are quite expensive to dispose of, making it a good feedstock to study its potential regarding thermochemical conversion into a fuel.

Supercritical water gasification (SCWG) of biomass is the gasification method that can achieve better results for high moisture content biomasses like BSG. With the help of the Aspen Plus® software, a model of a SCWG plant with a carbon capture unit was developed and coupled to another model of a combined cycle to simulate power production using the produced syngas as fuel.

Firstly a sensivity analysis was performed to check the influence of several parameters on the produced syngas characteristics. For high temperatures, a syngas with a hydrogen percentage of 66% can be reached, as opposed to a high percentage methane syngas (44.75%) obtained for low temperatures of just $400°C$.

As for LHV, high values ranging from 10.81 to 32.75 MJ/Nm^3 were obtained as the calculations were performed with an adjustment to not take into account the captured CO_2. Higher $LHVs$ were found, as expected, to correspond to syngases with higher CH_4 molar fractions. However, low gas yields were obtained for these syngases with high methane content and the opposite goes for hydrogen rich syngases. With these values, cold gas efficiency was calculated but results were disappointing, with a maximum value of 36.55% for the syngas produced at $900°C$, 241 bar and 5% feed concentration.

A point corresponding to close to optimal operating conditions, taking into account energetical and environmental costs of the process, and without making an exhausting study on the auxiliary consumptions and energy losses due to software limitations, was defined for 10% feed concentration and a temperature and pressure of gasification of $600°C$ and 241 bar, respectively.

The syngas produced was then used for the study of the combined cycle that was optimized by setting the temperature at the inlet of the gas turbine and the pressure ratio to the maximum. The air-to-fuel ratio selected was the stoichometric one, with a value of 22.13. Adiabatic flame temperatures of 2400.48 K were met for the combustion at atmospheric conditions.

Finally, 686.32 kW of work for a BSG feed rate of 1000 kg/h was obtained. This lead us to a good efficiency of the cycle (49.32%), but a quite low global efficiency of 16.6% due to the low cold gas efficiency, and to a negative emission factor of 574.95 $kgCO_2/MWh$.

Resumo

A biomassa é amplamente utilizada como fonte de energia para a produção de energia devido ao seu elevado poder calorífico, à sua disponibilidade a nível mundial e à sua pegada de carbono neutra.

Grandes quantidades de grãos usados da produção cervejeira (BSG) são obtidas em todo o mundo, sendo que a sua eliminação é bastante dispendiosa, fazendo com que seja um tipo de biomassa bastante interessante para estudar o seu potencial em termos de conversão termoquímica em combustível.

A gaseificação com água supercrítica (SCWG) é o método de gaseificação que permite obter melhores resultados para biomassas com elevado teor de humidade, como a BSG. Com a ajuda do software Aspen Plus®, foi desenvolvido um modelo de uma central SCWG com uma unidade de captura de carbono, acoplado a outro modelo de um ciclo combinado para simular a produção de eletricidade utilizando o gás sintético produzido como combustível.

Em primeiro lugar, foi efetuada uma análise de sensibilidade para verificar a influência de vários parâmetros nas características do gás sintético produzido. Para temperaturas elevadas, é possível obter um gás com uma percentagem de hidrogénio de 66%, por oposição a um gás sintético com uma elevada percentagem de metano (44.75%) obtido para temperaturas baixas de apenas $400°C$.

Quanto ao LHV, foram obtidos valores elevados, variando de 10.81 a 32.75 MJ/Nm^3, uma vez que os cálculos foram efectuados com um ajuste para não ter em conta o CO_2 capturado. Verificou-se que os $LHVs$ mais elevados, como esperado, correspondem a gases sintéticos com fracções molares de CH_4 mais elevadas. No entanto, foram obtidos baixos volumes de gás no caso de gases com elevado teor de metano e o oposto para gases sintéticos ricos em hidrogénio. Com estes valores foi calculada a eficiência do gás frio, mas os resultados foram decepcionantes, com um valor máximo de 36.55% para o gás sintético produzido a $900°C$, 241 bar e 5% de concentração de biomassa.

Um ponto correspondente às condições de funcionamento próximas das óptimas foi definido, tendo em conta os custos energéticos e ambientais do processo e sem fazer um estudo exaustivo dos consumos auxiliares e perdas de energia devido às limitações do software, para uma concentração de biomassa de 10% e uma temperatura e pressão de gaseificação de $600°C$ e 241 bar, respetivamente.

O gás sintético produzido foi então utilizado para o estudo do ciclo combinado, que foi optimizado definindo a temperatura à entrada da turbina a gás e a relação de pressão com o máximo valor possível. A relação ar/combustível selecionada foi a estequiométrica, com um valor de 22.13. Foram atingidas temperaturas adiabáticas de chama de 2400.48 K para a combustão em condições atmosféricas.

Finalmente, foram obtidos 686,32 kW de trabalho para 1000 kg/h de alimentação de biomassa. Isto conduziu-nos a uma boa eficiência do ciclo (49,32%), mas a uma eficiência global bastante

baixa de 16,6%, devido à baixa eficiência do gás frio, e a um fator de emissão negativo de 574,95 $kgCO_2/MWh$.

Acknowledgements

First and foremost, I am deeply thankful to my thesis supervisor, Prof. Eliseu Leandro de Magalhães Monteiro, for his unwavering support, expert guidance and time dispended in shaping the direction of this research.

I would like to extend my gratitude to the Faculty of Engineering of the University of Porto, for all the good moments and passed on knowledge of undisputed value that will benefit me for life.

I also feel the need to acknowledge the countless individuals whose work and research I have drawn upon for this thesis, for your invaluable contributions to the field.

To my family, to the ones that still walk this planet and the ones that are gone, a big heartfelt thanks for being my most precious treasure, my safe place and my guiding light that made me grow up and pull out the best of me.

Finally, I want to thank all my friends for always making me have a good time, specially to Ana Correia, Ana Soares and Ricardo Santos for always being up for a good laugh, even on times of trouble, and for all the time spent together that made us build an unbreakable connection between each other. Also a special thanks to my lovely girlfriend for motivating me and saving me from some stress during the development of this work.

Augusto Barbosa

"Considerar a nossa maior angústia como um incidente sem importância, não só na vida do universo mas da nossa mesma alma, é o princípio da sabedoria."

Fernando Pessoa

Contents

List of Figures

List of Tables

List of abbreviations and acronyms

BSG	Brewery's spent grains
CAPEX	Capital expenditure
CHP	Combined heat and power
daf	Dry and ash free
d.b	dry-basis
DCOALIGT	Model of Aspen Plus® (determination of densities for non-conventional components)
EU	European Union
EU-28	European Union consisting of 28 member states
GDP	Gross domestic product
HCOALGEN	Model of Aspen Plus® (determination of enthalpies for non-conventional components)
MIT	Massachusetts Institute of Technology
OPEX	Operational expenditure
PROXANAL	Proximate analysis in Aspen Plus®
PSA	Pressure swing adsorber
PVSA	Pressure vacuum swing adsorption
RKS-BM	Redlich-Kwong-Soave equation of state with Boston Mathias modifications
SCW	Supercritical water
SCWG	Supercritical water gasification
SS	Stainless steel
SULFANAL	Sulphur analysis in Aspen Plus®
ULTANAL	Ultimate analysis in Aspen Plus®
USA	United States of America
WGS	Water-gas shift
wt%	Weight percentage

List of variables

A/F	Air-to-fuel ratio	-
A/F_{st}	Stoichometric air-to-fuel ratio	-
a_{ij}	Number of atoms of element j in a mole of specie i	-
A_j	Total number of atoms of the element j	-
Ash	Biomass ash content	$\%$
b	Co-volume parameter	-
C	Carbon element	-
C_0	Initial carbon mass	kg
C_2H_4	Ethylene	-
C_2H_6	Ethane	-
C_i	Mole fraction of component i in the gas product	-
$Ca(OH)_2$	Calcium hydroxide	-
Cd	Cadmium	-
CGE	Cold gas efficiency	$\%$
CH_4	Methane	-
$C_xH_yO_z$	Generic organic compound chemical formula	-
CO	Carbon monoxide	-
CO_2	Carbon dioxide	-
COS	Carbonyl sulfide	-
d	Diameter of the heat-exchanger tube	m
d_i	Parameter calculated by the standard Soave formulation	-
$f.c.$	Feed concentration	$\%$
F_c	Carbon fraction of the biomass feed	-
FC	Biomass fixed carbon content	$\%$
f_i	Fugacity of specie$i$	Pa
f_i^0	Standard fugacity of specie i	Pa
G_i^0	Standard Gibbs free energy of specie i	J
G^t	Total Gibbs free energy of the system	J
H	Hydrogen element	-
H/C	Hydrogen to carbon ratio	-
H_2	Hydrogen	-
H_2O	Water	-
H_2S	Hydrogen sulfide	-
HCl	Hydrochloric acid	-
HCN	Hydrogen cyanide	-

HF	Hydrogen fluoride	-
Hg	Mercury	-
$H_{feed-in}$	Enthalpy of the feedstock through the heat exchanger	kJ
H_{gas-in}	Enthalpy of hot syngas through the heat exchanger	kJ
$H_{gas-out}$	Enthalpy of cold syngas through the heat exchanger	kJ
HHV	Higher heating value	kJ/kg
$HHV_{biomass}$	Higher heating value of the biomass	MJ/kg
k_g	Reaction rate constant	s^{-1}
K_2CO_3	Potassium carbonate	-
$KHCO_3$	Potassium bicarbonate	-
KOH	Potassium hydroxide	-
L	Lagrangian function	-
$LiOH$	Lithium hydroxide	-
LHV	Lower heating value	kJ/kg
LHV_{BSG}	Lower heating value of BSG	MJ/kg
LHV_{syngas}	Lower heating value of syngas	MJ/Nm^3
M	Biomass moisture content	$\%$
$\dot{m}_{air}$	Air mass flow	kg/h
$\dot{m}_{BSG}$	BSG mass flow	kg/h
$\dot{m}_{syngas}$	Syngas mass flow	kg/h
N	Nitrogen element	-
N_2	Nitrogen	-
$\dot{n}_{air}$	Molar flow of air	$kmol/h$
$NaCl$	Sodium chloride	-
$NaOH$	Sodium hydroxide	-
NH_3	Ammonia	-
n_i	Number of moles of specie i	mol
NO	Nitric oxide	-
$\dot{n}_{O_2}$	Molar flow of oxygen	$kmol/h$
NO_2	Nitrogen dioxide	-
NO_x	Nitrogen oxides	-
N_U	Nusselt number	-
O/C	Oxygen to carbon ratio	-
O	Oxygen element	-
p	Pressure	Pa
P_{AUX}	Auxiliary power consumption	W
p_b	Fluid-bulk thermal conductivity ratio	-
p_c	Critical pressure	Pa
PES	Primary energy savings	-
p_i	Pressure of specie i	Pa
p_i^0	Standard pressure of specie i	Pa
P_{losses}	Power from system losses	W
Pr_b	Prandtl number based on bulk fluid properties	-
p_w	Fluid-wall thermal conductivity ratio	-
r	Reaction rate	kg/s
R	Universal gas constant	$J/(K)$
Re_b	Reynolds number based on bulk fluid properties	-

S	Sulfur element	-
SO_2	Sulfur dioxide	-
SO_3	Sulfur trioxide	-
T	Temperature	$^{\circ}C$
T_c	Critical temperature	$^{\circ}C$
T_{sc}	Pseudo-critical temperature	$^{\circ}C$
V	Volume	m^3
$\dot{V}_{feed}$	Volume flow of the biomass feed	m^3/s
$\dot{V}_{syngas}$	Volume flow of the syngas	m^3/s
V_m	Molar volume	m^3/mol
VM	Biomass volatile matter	%
W_{Cgas}	Carbon flow rate in the product gas	kg/s
W_f	Reactor inlet feed rate	kg/s
$\dot{W}_{GT}$	Gas turbine work	W
W_p	Reactor outlet product rate	$kmol/s$
$\dot{W}_{ST}$	Steam turbine work	W
$\dot{W}_{total}$	Total combined cycle work	W
x	Length of the heat-exchanger tube	m
X_C	Mass fraction of carbon transformed into gas	-
X_{CH_4}	Molar fraction of methane	-
X_{CO}	Molar fraction of carbon monoxide	-
X_{H_2}	Molar fraction of hydrogen	-
Y	Carbon gasification yield	-
y_i	Molar fraction of specie i	-
z	Binary parameter	-
α_i	Carbon atoms in component i within the gas product	mol
$\Delta G^0_{f,i}$	Standard Gibbs free energy of formation of specie i	J
η_{CC}	Combined cycle efficiency	%
η_G	Global plant efficiency	%
η_{HX}	Heat-exchanger efficiency	%
μ	Lagrange multiplier	-
μ_i	Chemical potential of specie i	J/mol
τ	Reaction time	s
ϕ	Fugacity coefficient	-
$[H+][OH-]$	Ion product of water	$(mol/l)^2$

Chapter 1

Introduction

1.1 Relevance

In contemporary times, there exists significant political and societal pressure to mitigate the pollution stemming from industrial operations. The modern consumer demands rapid industrial output, which often results in substantial energy consumption and the generation of substantial waste materials [1]. A strategy embraced by industries to enhance efficiency involves repurposing their own waste and by-products to generate energy, aligning with the principles of a circular economy [2].

The brewing sector produces notable quantities of by-products with spent grains standing out as the most prevalent by-product, accounting for approximately 85% of the overall generated by-products. Spent grain generally makes up around 31% of the original malt weight [3], equivalent to roughly 20 kg/l of beer produced [4]. Notably, the brewing industry contributes around 1% to Portugal's GDP, resulting in the production of about 135,000 tons of brewery's spent grains (BSG) annually [5, 6].

Given BSG's rich content of sugars and proteins, the primary and most common approach for managing this industrial by-product has been its utilization as animal feed. Nevertheless, BSG presents itself as a promising raw material for diverse applications due to its economical nature, consistent year-round availability, and valuable chemical composition [5].

Biomass gasification has been gaining significant attention as a thermochemical recycling method, enabling the conversion of a diverse range of biomass and waste-derived materials into a syngas fuel. Supercritical water gasification is a well suited gasification process for BSG due to its high moisture content, since in this process water acts both as excellent reaction medium as a reactant due to its enhanced special properties in the supercritical state [7].

Due to the high pressures involved in this process, a more cost-effective and efficient carbon capture system can be implemented like the pressure swing adsorber [8]. This way, BSG can be converted into a high hydrogen content syngas that can be utilized for clean power production with a carbon-negative footprint [9]. For that, combined cycles are one of the best options since they

have improved efficiencies over the conventional Rankine and Brayton cycles, reaching up to 57% [10].

1.2 Objectives

This work is essentially focused on achieving a good performance from brewery´s spent grains biomass, after being converted into a syngas fuel with carbon capture included, in a combined gas and steam turbine cycle. To achieve that, Aspen Plus® software is used to develop two models corresponding to the supercritical water gasification and combined cycle plants, respectively, and they are coupled together in order to optimize the whole process of obtaining an efficient work output with extremely low CO_2 emission factor.

1.3 Structure

This dissertation is divided into 5 chapters, including this one, that serves as an introduction explaining the relevance and the main objectives of this work.

In chapter 2, firstly, some insights are given about the composition and obtention process for the brewery´s spent grains, as well as the potential applications of this feedstock. Secondly, a literature review on supercritical water gasification is made, explaining how can supercritical water benefit biomass gasification and going through a study on the several individual components of a supercritical water gasification plant and how the different parameters influence the performance of such process. This chapter finishes with some considerations about combined heat and power production cycles, how it works and its impact on the energy mix of Portugal and the European Union.

In chapter 3, it is explained the method used to simulate the supercritical water gasification process in Aspen Plus® and the validation of this model is realized by comparing some outputs of the process with the literature's. It is also shown the biomass feedstock used to proceed with this study.

Chapter 4 is related to the optimization of both the gasification of the biomass in study as well as the combined cycle performance when coupled to the supercritical water gasification plant. Here, several graphs showcasing the results obtained are plotted and a close to optimal point is selected.

Finally, in chapter 5, some conclusions regarding this study´s findings are written and future works are suggested.

Chapter 2

Supercritical water gasification of BSG

2.1 BSG: generation and composition

Barley stands as one of the world's most significant grains, following wheat, maize and rice. Its primary uses involve serving as animal fodder or as a foundational ingredient for beer production [11]. Barley kernels are notably abundant in starch and proteins, comprising three primary components: the germ (embryo), the endosperm (encompassing the aleurone and starchy endosperm), and the outer layers of the grain. The outer layers can be further categorized into three fractions: the seed coat, the layers immediately surrounding the aleurone and positioned above the seed coat are the pericarp layers, which are subsequently covered by the husk, as illustrated in figure 2.1 [12].

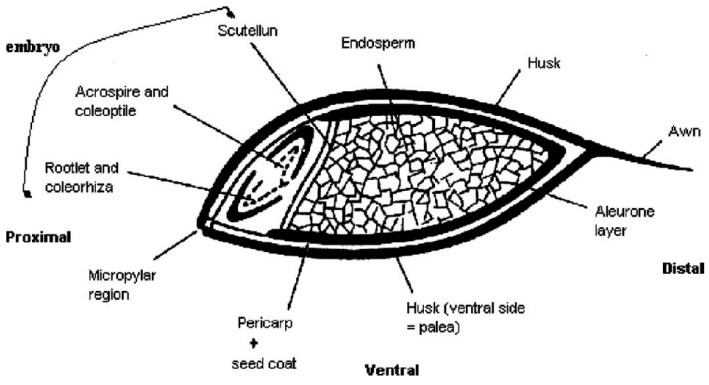

Figure 2.1: Scheme of a barley kernel [13]

To ready harvested barley for the brewing process, it undergoes cleaning and sorting based on its size. Following a resting period of 4–6 weeks, the barley undergoes controlled germination as part of the malting process, which aims to enhance the enzymatic composition of the grain. This malting procedure unfolds in the following sequence: steeping, germination, and subsequently drying or kilning [11, 14, 15, 16], as shown in figure 2.2.

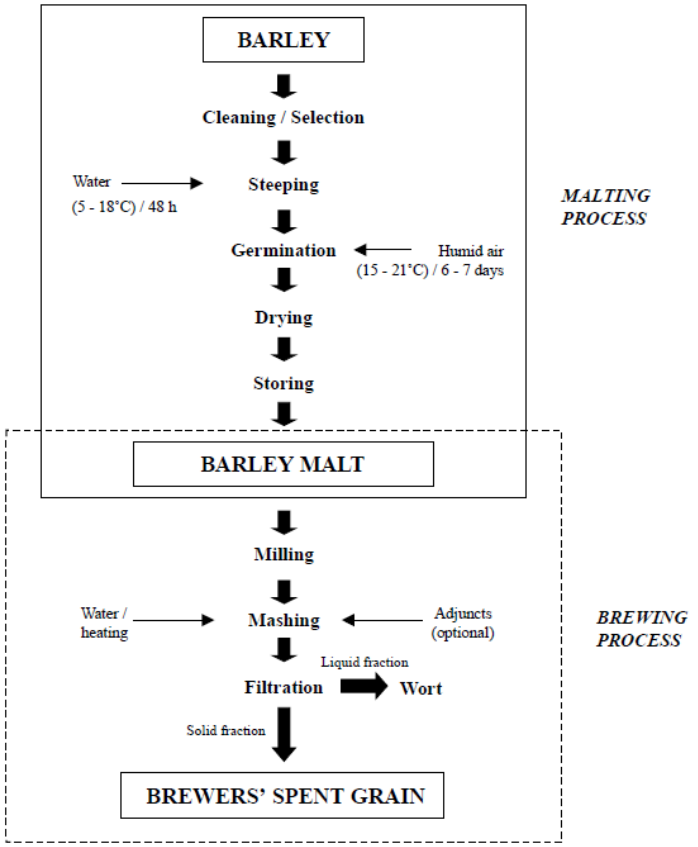

Figure 2.2: Representation of BSG obtention from barley [14]

BSG primarily encompasses the layers of husk, pericarp, and seed coat that envelop the original barley grain. This composite contains approximately 17% cellulose, 28% non-cellulosic polysaccharides, 28% lignin, along with traces of protein and lipids [14, 17]. Depending on the specific brewing process employed, there might be remnants of hops introduced during mashing. Notably, the husk harbors significant quantities of silica (constituting 25% of the mineral composition in barley as silicates) [12], along with trace amounts of calcium, iron, magnesium, phosphorus, potassium, sodium, etc., all present in concentrations below 0.5% [18], as we can verify in table 2.1.

The chemical makeup of BSG displays variation based on factors such as the variety of barley, harvest timing, and the conditions of malting and mashing [19, 20]. When compared to other by-products from agro-industrial processes, BSG showcases a lower cellulose content, yet its lignin content remains comparable [5]. This characteristic renders it suitable for use as a foundational material for the creation of valuable substances like activated charcoal, pesticides, fertilizers, polymers, and more [21]. Conversely, BSG boasts a notably elevated hemicellulose content, surpassing that found in various other by-products of agricultural crops. Protein levels within BSG are also considerably higher than those typically observed in other crop-derived by-products. The substantial presence of hemicellulose sugars and protein within BSG underscores its significant potential

for applications in both the food and biotechnological realms [5].

Table 2.1: Composition of BSG according to two studies

Item	**Meneses *et al* [22]**	**Mussato and Roberto *et al* [23]**
Components *(g/kg , d.b)*		
Cellulose	168	217
Hemicellulose	284	192
Xylan	199	136
Arabinan	85	56
Lignin	278	194
Acetyl groups	14	-
Proteins	153	247
Ashes	46	42
Extractives	58	107
Minerals *(mg/kg , d.b)*		
Silicon	10740	-
Phosphorus	5186	6000
Calcium	3515	3600
Magnesium	1958	1900
Sulfur	1980	2900
Potassium	258.1	600
Sodium	309.30	137.10
Iron	193.40	154.90
Zinc	178.00	82.10
Aluminium	36.00	81.20
Manganese	51.40	40.90
Cobalt	-	17.80
Copper	18.00	11.40
Strontium	12.70	10.40
Iodine	-	11.00
Barium	13.60	8.60
Chromium	5.90	< 0.50
Molybdenum	-	1.40
Boron	-	3.20

2.2 BSG for energy production

In recent times, BSG has garnered increased attention as a viable commodity due to the escalating costs associated with its disposal [24]. Given this context, various solutions have been

proposed for the utilization of BSG in energy generation. These alternatives encompass biogas production, ethanol synthesis, and thermochemical conversion processes such as pyrolysis, combustion, and gasification.

Biogas production from BSG is achievable through anaerobic digestion, resulting in a mixture primarily composed of 60–70% methane, accompanied by small proportions of hydrogen, nitrogen, carbon dioxide, and carbon monoxide [4, 25, 26]. Despite its high moisture content, BSG is suited for anaerobic digestion [27, 28]. However, the intermediate byproducts of lignocellulosic biodegradation hinder biogas production from BSG [27, 28]. The hydrolysis of fiber material within BSG represents a limiting step for the complete degradation process [14].

In recent years, ethanol has gained unprecedented attention due to its role as an alternative fuel to gasoline, rising oil prices, and its status as a sustainable energy source with environmental benefits. The global production of ethanol is currently at significant levels, largely relying on corn as the primary raw material. However, considering that this feedstock is essentially a food source, this scenario is still expected to evolve [29].

Among the potential pathways for energy generation from biomass like BSG, thermochemical conversion technologies such as combustion, pyrolysis, and gasification stand out. Thermal conversion processes operate relatively swiftly, taking minutes or seconds for completion, while biological processes relying on enzymatic reactions demand hours or even days. Consequently, for practical use, thermochemical conversion holds preference [7].

In the case of BSG combustion, pre-draining the spent grain to 55% moisture is necessary [30]. Nevertheless, BSG combustion leads to the emission of particles and toxic gases containing 1000 to 3000 mg/m^3 of nitrogen and 480 mg/m^3 of sulfur dioxide [30, 31]. The authors of [32] developed a process to create charcoal bricks from BSG. These charcoal bricks exhibited a high calorific value of around 27 MJ/kg, surpassing the original BSG and charcoals derived from other sources. According to [33], BSG charcoal consists of 81% fixed carbon and 12% ash. Thermal analysis revealed that BSG charcoal's combustion properties are inferior to those of sawdust charcoal, characterized by a higher ignition temperature and a longer burning duration.

Within the realm of thermochemical techniques, conventional gasification and plasma gasification are notable approaches with considerable potential for producing alternative fuels [24]. These methods hold promise not only from efficiency and economic perspectives but also in terms of environmental considerations [34].

2.3 Fundamentals of gasification

In recent times, gasification has garnered significant attention as an impactful thermochemical recycling method. This approach enables the conversion of a diverse range of biomass and waste-derived materials, including wood, plastics, municipal solid waste, as well as agricultural and industrial residues [35].

Table 2.2: Combustion and gasification products [35]

	Carbon	Hydrogen	Nitrogen	Sulfur	Others
Combustion	CO_2	H_2O	NO, NO_2	SO_2 or SO_3	Hg, Cd, HCl
Gasification	CO	H_2	HCN,N_2 or NH_3	H_2S or COS	

The resulting syngas is primarily composed of hydrogen (H_2), carbon monoxide (CO), carbon dioxide (CO_2), nitrogen (N_2), and certain low molecular weight hydrocarbons (CH_4, C_2H_4, C_2H_6, etc). Table 2.2 provides a comparative overview of the product gases obtained both from gasification and combustion processes.

As evident from the combustion process, the emission of hazardous substances into the environment is a concerning outcome. These include heavy metals such as mercury (Hg) or cadmium (Cd), as well as compounds like hydrogen chloride (HCl), sulfur dioxide (SO_2), nitrogen oxides (NO_x) and hydrogen fluoride (HF) [36]. In contrast, during the gasification process, the production of potentially harmful compounds is notably minimal, consisting of small quantities of hydrogen sulfide (H_2S), and ammonia (NH_3). Tar and char may also be produced [37]. Furthermore, gas separation techniques can be employed to eliminate carbon dioxide (CO_2) from the syngas stream [7, 36]. Tar, a complex blend of condensable hydrocarbons encompassing aromatics, polyaromatics, and linear organic compounds [38, 39], poses a significant challenge due to its association with the formation of carcinogenic substances, process disruption, and catalyst deactivation [40].

Currently, the primary source of syngas production remains coal. As described in [41], approximately 6 exajoules (EJ) of syngas are generated annually. This syngas finds diverse applications, as depicted in the diagram below:

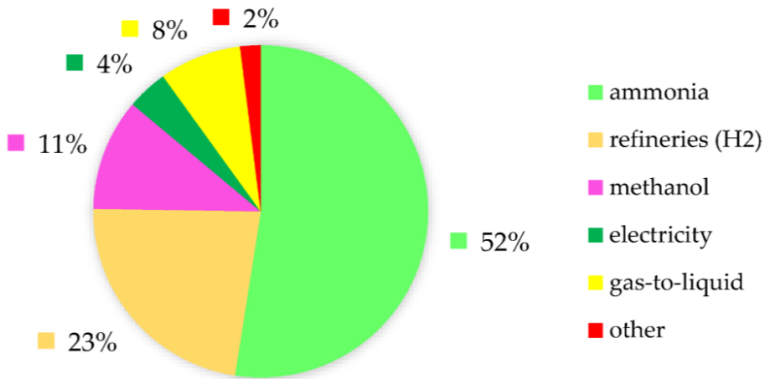

Figure 2.3: End use of Syngas [41]

Various gasification processes can be classified based on the gasifying agent employed. These include air gasification, oxygen gasification, steam gasification, carbon dioxide gasification, supercritical water gasification, and more. In general, oxygen, steam, carbon dioxide, and supercritical water gasification tend to yield higher heating values (HHVs) of syngas compared to air gasification. However, despite the higher energy potential in these alternatives, air gasification remains

the most extensively studied and experimentally utilized technique [36].

2.4 Supercritical water gasification (SCWG)

During the mid-1970s, Sanjay Amin, a graduate student at the MIT, was investigating the decomposition of organic compounds through steam reforming in hot water. In the course of his experiment with subcritical water, he observed the substantial production of char and tars. Interestingly, when he elevated the water's temperature above its "critical state," he noticed that the tar formed in the subcritical phase completely vanished [42].

Thermal gasification utilizing air, oxygen, or subcritical steam as the gasification medium, proves highly efficient for dry biomass. However, it becomes notably inefficient when dealing with high-moisture biomass. This inefficiency stems from the substantial requirement to eliminate moisture before the thermal gasification process can commence, which consumes a significant amount of additional energy (2242 $kJ/kg_{moisture}$) for its evaporation. Consequently, for gasifying highly wet biomass, hydrothermal gasification performed in high-pressure hot water emerges as a more favorable approach. Unlike thermal gasification, water in hydrothermal processes is not a hindrance but rather serves as both a reaction medium and a reactant [7].

The effectiveness of hydrothermal processes remains consistent regardless of the biomass's moisture content. It was found out that the gasification efficiency remained nearly unaltered at 31% and 51%, respectively, even when the biomass's moisture content ranged from 5% to 75% [43].

Supercritical water has garnered significant interest due to its distinct attributes, offering rapid biomass hydrolysis, high solubility of intermediate reaction products, and a high ion product slightly below the critical point that enhances ionic reactions [7].

The appeal of SCWG for large-scale applications has grown in line with the increased emphasis on generating cost-effective and environmentally friendly "green" hydrogen [7].

2.4.1 Supercritical water

As temperature increases, the pressure needed for water to maintain its liquid phase also rises. Beyond a critical point, the boundary that separates the two phases ceases to exist, effectively eliminating the distinction between liquid and vapor phases. The temperature and pressure at this specific juncture are referred to as the critical temperature (374.21$°C$) and critical pressure (22.089 MPa), respectively, as seen on figure 2.4.

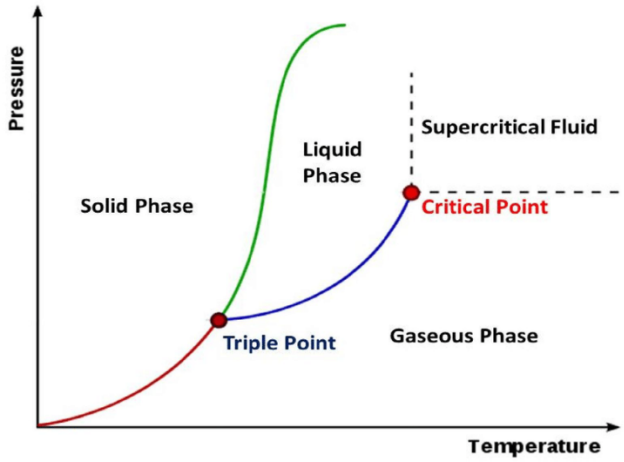

Figure 2.4: Water phase diagram showcasing the critical point [44]

When subjected to temperatures above its critical pressure, water undergoes a continuous shift from a state resembling a liquid to one resembling a vapor. Unlike the subcritical stage, this transition from liquid-like to vapor-like does not necessitate the input of heat for vaporization.

Nonetheless, there exists a temperature known as the pseudo-critical temperature for each pressure above the critical pressure at which the transition from liquid-like to vapor-like occurs. This temperature is characterized by a noticeable increase in the specific heat of the fluid [7]. An empirical equation can be employed to estimate this temperature with approximately 1% accuracy [45]:

$$\begin{aligned} T^* &= (p*)^F \\ F &= 0.1248 + 0.01424p* - 0.0026(p*)^2 \\ T^* &= \frac{T_{sc}}{T_c}, \; p^* = \frac{p}{p_c} \end{aligned} \tag{2.1}$$

where p_c and T_c are the critical pressure and critical temperature of water, respectively, and T_{sc} is the pseudocritical temperature at a pressure $p > p_c$.

2.4.1.1 Properties of supercritical water

The critical point represents a significant turning point in the thermophysical characteristics of water. Notably, there's a distinct surge in specific heat close to the critical temperature, followed by a similar decline, as depicted in figure 2.5. The peak value of specific heat decreases in correspondence with system pressure. In the realm of thermal conductivity, water's value drops from 0.330 W/K at 400°C to 0.176 W/mK at 425°C. While viscosity experiences a notable reduction, it increases with temperature beyond the critical point [7]. Regarding density, the change across supercritical water (SCW) and its pseudo-critical temperature is relatively modest, shifting from approximately 1000 to 200 kg/m^3, as shown in figure 2.6. This, coupled with its low viscosity, minimal surface tension, and heightened diffusivity, significantly contributes to SCW's

exceptional transport properties [7]. These properties facilitate its effective and rapid infiltration into the pores of biomass for efficient reactions.

Furthermore, when water surpasses its critical point, it undergoes a marked transformation in its solvent nature primarily due to the reduction in hydrogen bonding [7]. The dielectric constant of water experiences a decline from around 80 under ambient conditions to about 10 at the critical point, as illustrated on figure 2.5. In proximity to its critical point, water showcases higher ion products ($[H+][OH-] \sim 10^{-11}\ (mol/l)^2$) compared to its subcritical state under ambient conditions ($\sim 10^{-14}\ (mol/l)^2$), as seen in figure 2.6. Consequently, water becomes an effective medium for acid or base-catalyzed organic reactions [46]. However, beyond the critical point, the ion product diminishes sharply ($\sim 10^{-24}\ (mol/l)^2$), causing water to transition from a highly polar solvent in ambient conditions to a nonpolar solvent. This transformation positions SCW as an excellent solvent for non-polar organic compounds [7, 47], such as lignin. Conversely, it becomes a less suitable solvent for strongly polar inorganic salts, simplifying the separation of salts and gases from the product mixture within an SCW gasifier.

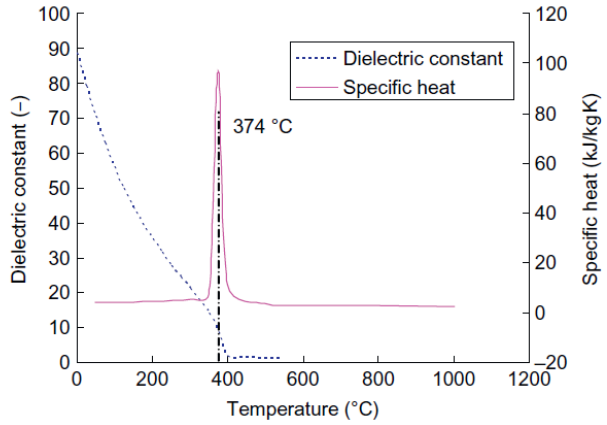

Figure 2.5: Dielectric constant and specific heat of water variation with temperature [7]

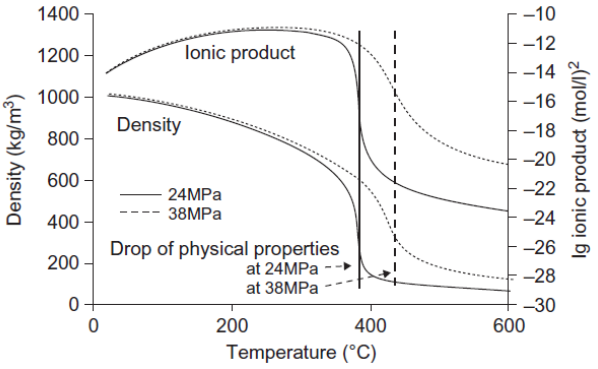

Figure 2.6: Water´s density and ionic product evolution with temperature for two different pressures [7]

2.5 Biomass SCWG process

The process of supercritical water gasification of biomass is conventionally conducted within the temperature range of 600 to 650°C, under a pressure approximately around 30 MPa. Beyond 600°C, water takes on the role of a potent oxidizing agent. Carbon atoms undergo oxidation, favoring the formation of carbon dioxide (CO_2). Furthermore, the presence of water contributes to a substantial yield of hydrogen. Notably, hydrogen atoms are not only sourced from the biomass itself but also from water, collectively forming hydrogen [48].

An overarching chemical reaction that encapsulates the biomass supercritical water gasification process can be outlined as follows [7]:

$$CH_xO_y + (2-y)H_2O \rightarrow CO_2 + (2y + x/2)H_2 \tag{2.2}$$

In the provided reaction equation, the variables x and y represent the molar ratios of hydrogen to carbon (H/C) and oxygen to carbon (O/C) in the biomass, respectively. The outcome of this reaction is the generation of syngas. The primary thermochemical reactions integral to SCWG are as follows [49]:

- Steam reforming reaction 1 :

$$C_xH_yO_z + (2x-z)H_2O \rightarrow xCO_2 + (2x - z + y/2)H_2 \tag{2.3}$$

- Steam reforming reaction 2 :

$$C_xH_yO_z + (x-z)H_2O \rightarrow xCO + (x - z + y/2)H_2 \tag{2.4}$$

- Water gas shift (WGS) reaction :

$$CO + H_2O \rightarrow H_2 + CO_2 \tag{2.5}$$

- Methanation reaction of CO_2 :

$$CO_2 + 4H_2 \rightarrow CH_4 + 2H_2O \tag{2.6}$$

- Methanation reaction of CO :

$$CO + 3H_2 \rightarrow CH_4 + H_2O \tag{2.7}$$

Over the last 15 years, research in the field of SCWG has transitioned from focusing on simplified model compounds to incorporating actual lignocellulosic biomass sources. This shift signifies a move towards utilizing authentic materials such as agricultural residues, forestry biomass, and industrial biomass waste [50]. However, it's worth noting that SCWG of genuine biomass presents

heightened challenges owing to the intricate composition of real biomass feedstock and the simultaneous occurrence of multiple reactions in both solid and liquid phases [51].

2.6 SCWG process variables

2.6.1 The effect of temperature on the gasification efficiency

Temperature plays a pivotal role in shaping both the distribution of products and the efficiency of the supercritical water gasification process. The efficiency of gasification is typically quantified in terms of the hydrogen or carbon content present in the gaseous phase as a fraction of the original biomass content. As temperature increases, the overall carbon conversion and hydrogen yield experience an augmentation due to the chemical breakdown of heavy hydrocarbons. This phenomenon promotes a higher molar fraction of permanent gases like H_2 and CO at elevated temperatures [52], leading to decreased yields of methane, tar, and char. While it's generally advisable to operate at temperatures above 800°C to mitigate tar formation [53], such high temperatures can lead to a greater oxidation of the feedstock, resulting in a reduction of the syngas's chemical energy and promoting slag formation.

The higher gas production at elevated temperatures can be attributed to the greater release of gases during the initial devolatilization phase, as well as the secondary reactions undergone by char and tar (char gasification and tar cracking/reforming) [53]. The study conducted on [54] highlighted that increasing the temperature from 1000 to 1350°C led to a remarkable 72% increase in gas yield.

As depicted in figure 3.5, the hydrogen yield demonstrates an exponential rise above 600°C. Meanwhile, the CO yield starts to decline above 600°C due to the initiation of the shift reaction (Eq. 2.5). Carbon conversion efficiency displays a steady increase with temperature, nearly reaching 100% beyond 700°C. Hydrogen conversion efficiency also follows an ascending trend with temperature. Interestingly, at 740°C, the hydrogen conversion efficiency surpasses 100%, reaching 158%. This observation clearly underscores that the additional hydrogen originates from water, affirming its role not only as a reaction medium but also as a reactant within the SCWG process [7].

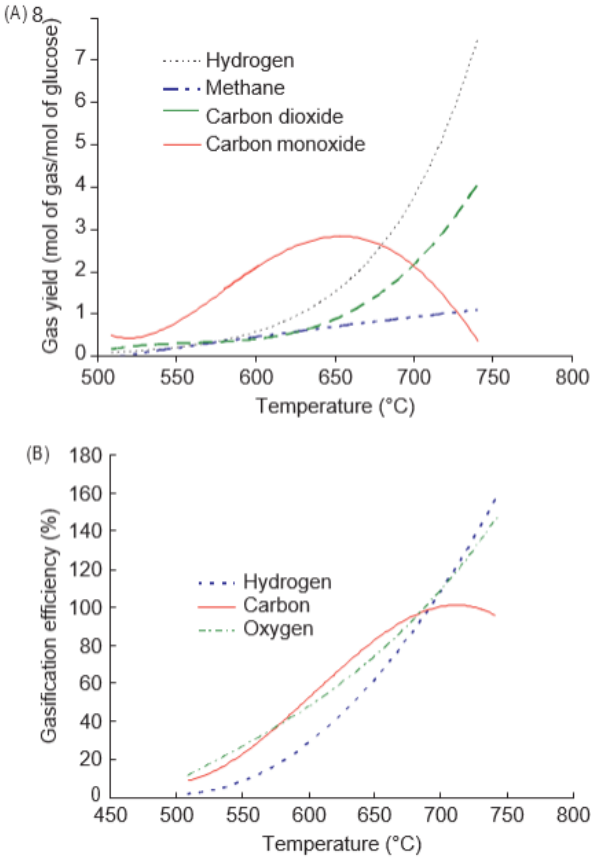

Figure 2.7: Gas yields and gasification efficiency evolution with temperature [55]

2.6.2 The effect of reaction/residence time on the gasification efficiency

The duration of the reaction is another variable that exerts a direct influence on gasification efficiency and the yields of specific gases.

The reaction rate, denoted as r, is quantified as the reduction in the fraction of biomass carbon, represented as C, over time. Assuming a scenario of pseudo-first-order kinetics, the relationship can be expressed as follows [7]:

$$r = -\frac{dC}{d\tau} = k_g C \tag{2.8}$$

where k_g is the reaction rate constant.

The proportion of carbon transformed into gas, denoted as Xc, can be correlated to the present carbon fraction, C, and the initial carbon fraction, C_0, within the fuel, using the following relationship:

$$X_c = 1 - \frac{C}{C_0} \tag{2.9}$$

Now replacing the carbon fraction in Eq.2.8 and integrating, we get:

$$k_g = -\frac{ln(1-X_c)}{\tau} \tag{2.10}$$

Gasification efficiency and hydrogen yields typically exhibit an increase with prolonged reaction time due to the prevalence of thermal cracking reactions encompassing processes like dehydration, decomposition, decarboxylation, and depolymerization [56]. At shorter reaction durations, the effectiveness of hydrothermal liquefaction grows, liquefying reactive constituents to produce more stable components like acetic acid and methanol [57]. Over extended timeframes, hydrogen generation is feasible, albeit a peak production point exists contingent on the feedstock's nature. Following this peak, methanation reactions, which consume hydrogen, tend to gain prominence, leading to a decrease in hydrogen yield [57, 58]. The decline in carbon monoxide yield over lengthier reactions suggests an inclination towards water-gas shift (WGS) reactions and methanation reactions.

In batch-mode SCWG experiments, reported reaction times generally span from minutes to tens of minutes, whereas continuous-mode SCWG studies typically cite reaction times in the range of tens of seconds [59, 60].

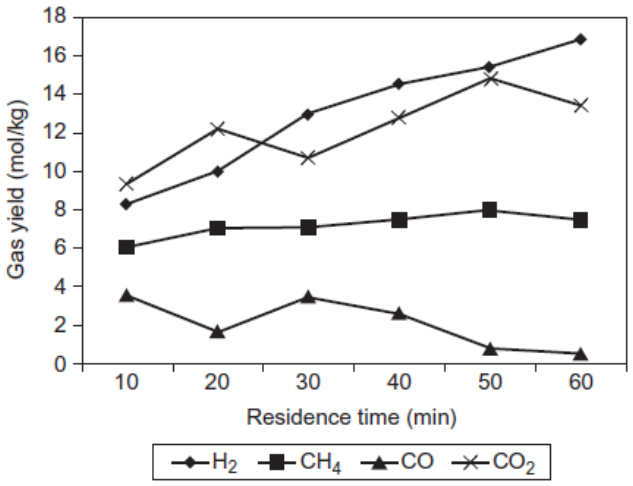

Figure 2.8: Gas yield evolution with residence time for the SCWG of 2% rice husk at 650°*C* and 30 *MPa* [7]

2.6.3 The effect of pressure on the gasification efficiency

A limited number of SCWG investigations involving real biomass have explored the impact of pressure on hydrogen yield. In a continuous SCWG study involving wood sawdust [59] , it was observed that hydrogen yields escalated as the pressure increased, ranging from 17 to 30 *MPa*, concurrent with reductions in yields of CH_4 and *CO* at a temperature of 650°*C*. This trend indicates that higher pressures contribute to the elevation of hydrogen yields while concurrently suppressing CH_4 and *CO* yields.

It's important to note that elevated pressure fosters a favorable environment for ionic reactions due to the ion stabilization effect generated by the heightened water density. Conversely, radical reactions tend to be less favored under these conditions. However, there are inherent challenges related to capital expenditure (CAPEX) and operational expenditure (OPEX) costs when designing a system that can safely operate at elevated pressures [50].

2.6.4 The effect of biomass composition on the gasification efficiency

A majority of the studies concur that biomass containing higher amounts of cellulose and hemicellulose undergoes more facile gasification [61]. Specifically, cellulose tends to contribute more significantly to hydrogen yield compared to hemicellulose and lignin. Furthermore, the influence of lignin on gas yields is less pronounced, particularly at temperatures surpassing $600°C$, when a catalyst is utilized. This is attributed to the enhanced capability to gasify lignin in the presence of a catalyst [50].

2.6.4.1 The effect of feedstock concentration/biomass-to-water mass ratio on the gasification efficiency

In the context of supercritical water gasification, water assumes a dual role as both a reactant and a reaction medium. When the water content decreases relative to the concentration of the feedstock, it effectively restrains the progression of these reactions. Consequently, this reduction in water content has the potential to hinder the generation of hydrogen yields [62, 63].

Thermodynamic calculations indicate that the conversion of carbon to gases in SCW experiences a rapid decline when the solid content in a liquid feed surpasses 50% [64]. Experimental data further support this, with observations from the studies on [65, 66] revealing that gasification efficiency commences its descent when the solid concentration exceeds even a modest 2%. This situation necessitates higher pumping expenses and liquid effluent management, which could pose substantial challenges to the commercial viability of SCWG.

Furthermore, the type of reactor employed also plays a role in how solid concentration influences gasification efficiency. For instance, the study in [67] noted that a stirred reactor exhibits elevated gasification efficiency at higher solid content in the feed. Stirred reactors facilitate thorough mixing of reactants, resulting in a heating rate that surpasses that achieved in other reactor types.

2.6.4.2 Feed particle size

The influence of biomass particle size is an area that lacks extensive research. Available data is limited, but data in [59] demonstrated that smaller particles tend to yield a slightly enhanced hydrogen yield and increased gasification efficiency. However, in contrast, the study in [65] in

did not observe any discernible effect when they experimented with varying the size of rice husk particles within the range of 1.25 to 0.5 *mm*.

Furthermore, even if the impact of particle size is substantiated through more comprehensive studies, the question arises as to whether the additional energy required for grinding the biomass is justified by the observed improvement in outcomes [7]. This consideration underscores the need to balance energy input and process efficiency when evaluating the potential benefits of altering particle size.

2.7 SCW plant design

A typical SCWG plant comprises several essential components as outlined below [7] (refer to figure 2.9 for visualization):

- Feedstock pumping system: biomass is transformed into a slurry suitable for feeding into the gasifier. It is then pumped to achieve the required supercritical pressure. Alternatively, water can be pressurized independently, and the biomass subsequently introduced into it;
- Feed preheater: the feedstock, regardless of whether biomass or water is pressurized, needs to be heated to the predetermined inlet temperature for the gasifier. This temperature must exceed the critical temperature of water;
- Gasifier/Reactor: this is the core component where gasification takes place. Biomass undergoes a series of chemical reactions under SCW conditions, leading to the production of syngas;
- Heat-Exchanger: a portion of the sensible heat from the gasification product is reclaimed in a waste heat-recovery exchanger. This recovered heat can be utilized for partially preheating the incoming feed;
- Gas-Liquid separator: following gasification, the product is initially cooled in the waste heat-recovery unit. Subsequently, it undergoes further cooling to reach ambient temperature through an external heat exchanger connected to a coolant. The low solubility of hydrogen and methane in water at high pressure and low temperature results in their separation from water after cooling. Carbon dioxide, with its high solubility in water, remains in the liquid phase;
- Product-Upgrading equipment (optional): depending on the desired end products, additional equipment may be incorporated for further processing or upgrading of the gasification products. For example, to segregate the gaseous hydrogen from methane, a pressure swing adsorber is utilized. Subsequently, the CO_2-rich liquid is depressurized to atmospheric pressure, causing separation of carbon dioxide from water and unconverted salts.

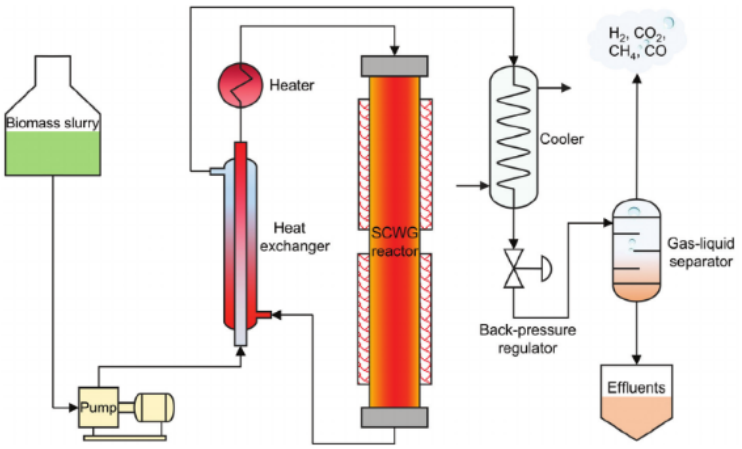

Figure 2.9: Scheme of a typical SCWG plant [68]

2.7.1 Reactors

The principal design parameters for an SCWG reactor encompass temperature, reaction time, pressure, catalyst utilization and feed concentration. These parameters collectively govern the performance and outcomes of the SCWG process [7].

2.7.1.1 Reactor type

SCWG reactors are either configured as batch or continuous flow. Continuous reactors are commonly tubular reactors or fluidized bed reactors. In contrast, batch reactors are often autoclaves with volumes ranging from a few milliliters to a liter. The type of reactor plays a significant role in how feed concentration influences the process [7].

Batch reactors offer simplicity and don't necessitate high-pressure pumps, making them suitable for a wide array of biomass feedstocks. However, their reaction processes are non-isothermal, requiring time for both heating up and cooling down. During the heating-up phase, various reactions occur, leading to transformations in the feedstock [7]. In batch processes, biomass and water components are sealed inside an autoclave reactor and stirred using an agitator. Fixed-volume cells enable the isolation of operating parameters and the effects of diverse catalysts. On the other hand, continuous-flow reactors can make it more challenging to separate and isolate operating variables [50].

While there's limited evidence in the literature regarding the feasibility of scaling up the SCWG process using batch reactors, challenges persist with continuous flow reactors. These challenges pertain to optimizing hydrogen production efficiency, minimizing char formation, addressing reactor corrosion, and preventing plugging issues [69, 70, 71].

2.7.1.2 Reactor temperature

In supercritical water gasification , the operational conditions must surpass the critical values of 374.21°C and 22.089 MPa for temperature and pressure, respectively. Designing the reactor with a lower temperature offers advantages in terms of reduced energy requirements for feed preheating, enhancing overall process efficiency. However, the gasification temperature needs to be maintained above 600°C to achieve a satisfactory hydrogen yield. This requirement can potentially be lowered when catalysts are incorporated [7].

For the production of synthetic natural gas, specific composition requirements include high methane levels and low hydrogen content. In such cases, a reaction temperature ranging from 350°C (just below the critical point) to 500°C can be chosen [7]. However, this lower temperature range necessitates the use of catalysts to achieve reasonable yield levels, as highlighted in the study [72].

2.7.1.3 Catalyst selection

The selection of a catalyst holds sway over reactor temperature, the distribution of products, and the potential for plugging. In the realm of supercritical water gasification, catalysts assume a pivotal role in efficiently generating hydrogen, especially considering the inherently high activation energies associated with SCWG reactions [7].

Catalysts have the capacity to significantly enhance biomass conversion even at lower temperatures, thereby mitigating both capital and operational costs of the process. Opting for operation at higher temperatures necessitates the use of premium heat-resistant and corrosion-resistant materials like *Inconel* 625 for tubing and fittings, which can escalate expenses in comparison to employing lower-temperature materials like *SS* 316 [50, 73]. Furthermore, heating costs for non-catalytic SCWG at 600°C significantly surpass those for catalytic SCWG at 400°C, as it is demonstrated on table 2.3. By strategically leveraging catalysts, SCWG processes can optimize efficiency, reduce costs, and enhance the overall feasibility of the operation.

Table 2.3: Aspen Plus® economical analysis simulation for catalytic and non-catalytic SCWG [50]

Parameters	**400°C (catalytic)**	**600°C (non-catalytic)**
Total CAPEX (USD)	6,037,450	7,823,040
Total OPEX (USD)	7,817,240	9,500,360
Total raw material cost ($USD/year$)	4,295,390	5,384,810
Total utilities cost ($USD/year$)	466,542	888,246
Electricity (kW)	300.74	302.23

Alkali catalysts (such as $Ca(OH)_2$, KOH, $KHCO_3$, K_2CO_3, $LiOH$, $NaOH$, $NaCl$, etc) are frequently employed homogeneous catalysts in SCWG. They effectively lower the initial temperature

necessary for cellulose degradation and accelerate the water-gas shift reaction, leading to increased yields of hydrogen and CO_2, while simultaneously reducing CO production [74, 75]. However, the recovery of homogeneous catalysts poses challenges, adding to ongoing costs due to the need for fresh catalyst addition. Additionally, the liquid waste containing alkali catalyst generated after SCWG is problematic to treat [63, 76], further dampening the attractiveness of alkali catalysts.

Consequently, many researchers have shifted their focus towards heterogeneous catalysts due to their more feasible recovery and cost-effectiveness [50]. Particularly, metal-supported heterogeneous catalysts have demonstrated improved hydrogen yield, especially in single-use batch experiments [57, 75, 77, 78]. Nickel-catalysts are known for promoting essential reactions like the WGS, methanation, and hydrogenation, playing a vital role in hydrogen production and CO elimination [76]. While some studies suggest that ruthenium might be slightly more active than nickel [57, 76], it generally doesn't yield higher hydrogen production than nickel-based supported catalysts, and its higher cost discourages its widespread use [79].

The choice of the support material significantly impacts catalyst performance. Natural mineral catalysts like trona, borax, dolomite and olivine have gained attention for their benefits, including low cost, widespread availability, and the advantage of not requiring elaborate recovery processes [71, 74, 80, 81, 82]. These natural mineral catalysts have shown promise for enhancing hydrogen yield in SCWG processes while circumventing some of the challenges associated with traditional alkali catalysts.

2.7.1.4 Reactor size

Let's assume a reactor that takes in a feed rate of W_f (kg/s) and generates a product rate of W_p $(kmol/s)$. This product encompasses various hydrocarbon constituents denoted by the species i. Then we can calculate the carbon flow rate in the product gas (W_{Cgas}) as [7]:

$$W_{Cgas} = \sum W_p C_i \alpha_i (kmol/s) \tag{2.11}$$

where in this context α_i represents the count of carbon atoms in component i within the gas product, C_i signifies the mole fraction of component i in the gas product and W_p denotes the flow rate of the product gas. The quantity of carbon present in the feed can be determined by considering W_f, along with its carbon fraction, denoted as F_c.

The carbon gasification yield, denoted as Y, is defined as the proportion of carbon that has undergone gasification in relation to the total carbon content present in the feed [7]:

$$Y = \frac{\sum_i 12 W_p \alpha_i C_i}{W_f F_c} = \frac{12 W_{Cgas}}{W_f F_c} \tag{2.12}$$

where 12 is the value of the carbon's molecular weight $(kg/kmol)$. Recovering the reaction time (τ) from Eq. (2.10) we can write for a continuous stirred-tank reactor:

$$\tau = \frac{V}{\dot{V}_{feed}} \tag{2.13}$$

and so, given a known reaction rate, k_g, and a desired conversion, X_c (related to τ in Eq.2.10), we can estimate the volume of the reactor needed for the gasification process.

2.7.2 Heat-recovery heat-exchanger

A feedstock preheater holds the position of the second most crucial component within an SCWG system. The energy required to elevate the temperature of the feedstock to the desired level is a substantial portion of the potential heating value contained within the resultant product gas. In the absence of an effective recuperation of heat from the product gas, the external energy needed for the gasification process might surpass the energy output, turning the gasifier into a net consumer of energy. Consequently, it becomes essential for the feedstock to harness the maximum possible thermal energy from the sensible heat inherent in the product [7]. The most common heat-exchanger types are the shell-and-tube and plate configurations but the *Matsumura* group developed a spiral type coupled with a spiral reactor with good results [83].

The efficiency of heat exchange, denoted as η_{HX}, quantifies the proportion of the available heat in the product stream that can be transferred to the feed stream. This parameter signifies how effectively the heat present in the product gas can be utilized to preheat the incoming feedstock [7],

$$\eta_{HX} = \frac{H_{gas-out} - H_{gas-in}}{H_{feed-in} - H_{gas-in}} \tag{2.14}$$

where H represents the enthalpy of the system.

This efficiency has a strong relationship with surface area where heat transfer occurs and feed pressure, as illustrated by figure 2.10.

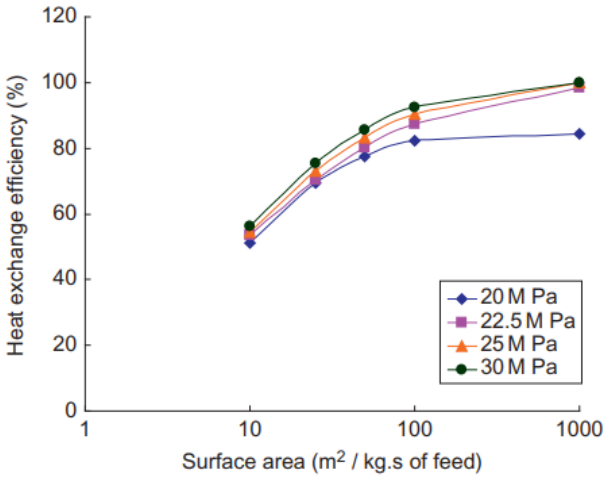

Figure 2.10: Heat exchange efficiency relationship with surface area and feed pressure [7]

Notably, the heat-recovery exchanger emerges as a significant contributor, accounting for approximately 50-60% of the total capital expenditure for the entire plant [84]. This underscores the critical importance of the heat-recovery exchanger as a pivotal component within the SCWG system due to its substantial financial impact. Figure 2.11 provides a comparison of the capital costs associated with various components/processes of an SCWG plant.

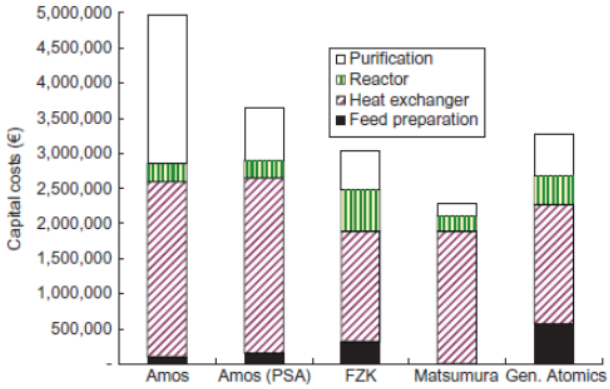

Figure 2.11: CAPEX of each component or process of a SCWG plant [84]

2.7.2.1 Heat transfer considerations for SCW conditions

In supercritical water, the thermal conductivity is notably lower compared to its subcritical counterpart, exhibiting a rapid decline as temperature increases. The heat-transfer coefficient, on the other hand, demonstrates variation in proximity to its pseudocritical value, with both conductivity and viscosity experiencing a decrease, while specific heat encounters an increase. All this contributes to an enhanced overall heat-transfer rate. However, as temperature continues to rise beyond this point, both specific heat and thermal conductivity diminish, consequently leading to a reduction in the heat-transfer coefficient. Typically, under conditions of high heat flux and low mass flux, the heat transfer tends to deteriorate, ultimately resulting in localized areas of elevated temperature, commonly referred to as "hot spots," within the tubing system [7]. The fluid-to-wall heat-transfer coefficient in a vertical tube, within the context of supercritical water conditions, may be calculated by the following correlation [85]:

$$N_u = 0.061 Re_b^{0.904} Pr_b^{-0.684} \left(\frac{p_w}{p_b}\right)^{0.564} \tag{2.15}$$

Drawing from a comprehensive analysis of experiments and evaluations encompassing 15 correlations,the subsequent correlations were proposed as preferable options for horizontal tubes [86]:

$$N_u = 0.0069 Re_b^{0.9} Pr_b^{-0.66} \left(\frac{p_w}{p_b}\right)^{0.43} \left(1 + \frac{2.4}{x/d}\right) \tag{2.16}$$

where x is the length and d the diameter of tube. Heat transfer in SCWG may vary because of solids in the fluid. Thus, applicability of these equations to SCWG is uncertain [7].

2.7.3 Carbon combustion system

The gasification and pyrolysis reactions involved in the process are characterized by their endothermic nature, necessitating an external heat source to sustain the reactor's operation. Conventionally, a fraction of the hydrocarbon or carbon within the feed is allowed to undergo combustion within the gasifier, albeit resulting in energy loss from the feedstock. In contrast, an SCW gasifier operates at significantly lower temperatures, thereby demanding less heat input. In terms of thermodynamics, the recovered heat from the gasification product is insufficient to elevate the feed to the requisite gasification temperature. To bridge this energy gap, external sources of heat or combustion of a portion of the product gas in a heater are typically employed, both of which involve substantial costs. A more desirable solution would involve the controlled combustion of the minor quantities of unconverted char located upstream of the gasifier, effectively enabling SCWG to achieve energy self-sufficiency. This approach to char combustion also offers an additional advantage in cases where solid catalysts are used in SCWG, as these catalysts can become deactivated when coated with unconverted char within the gasifier. The heat generated through char combustion is conveyed to the gasifier through both the solid catalysts and the gasifying medium (comprising SCW and CO_2) [7].

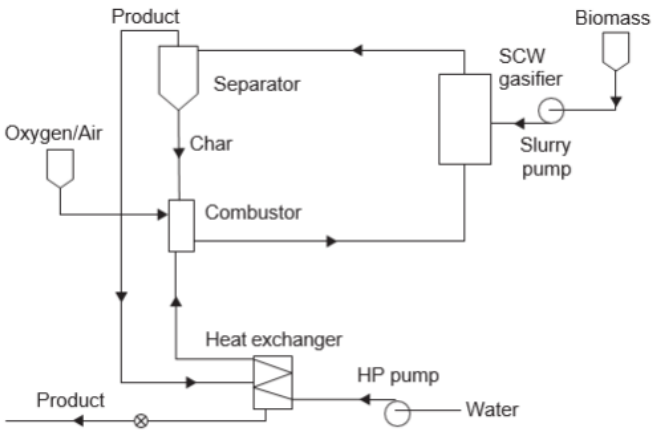

Figure 2.12: Example of a carbon combustion system integration within a SCWG plant [7]

2.7.4 Gas-liquid separator and carbon capture systems

In an SCWG system, the process of separating the product gas mixture from water is usually carried out in two distinct stages: the first stage involves an initial separation in a high-pressure but low-temperature separator. The second stage is where the final separation occurs, and it takes place under conditions of both low pressure and low temperature [7].

At relatively low temperatures ranging from 25 to 100°C, gases like H_2 and CH_4 exhibit very low solubility in water, even when subjected to high pressures. This unique characteristic can be utilized to effectively separate these gases from CO_2. However, it's important to note that the equilibrium concentration of CO_2 may not be sufficient to dissolve the entire quantity of CO_2 present in the high-pressure water. To achieve complete separation, additional water might need to be introduced into the system. This additional water requirement is expressed as the ratio of water to gaseous product (denoted as R) on a weight basis. The relationship between pressure, R, and the composition of the separated gases plays a pivotal role in this separation process. Increasing pressure and the value of R enhances the purification of H_2, but this comes at the cost of decreasing the concentration of hydrogen in the gas phase. Thus, by adjusting the pressure and R, it's possible to either recover a higher quantity of H_2 with lower purity, or a smaller quantity of highly pure H_2, depending on the specific requirements [7].

After the initial phase of separation, it becomes viable to implement a carbon capture procedure. Power facilities powered by biomass are inherently balanced in terms of carbon emissions. Thus, the incorporation of a carbon capture system into a plant is anticipated to result in the production of energy with a carbon-negative footprint [9]. A pressure swing adsorber system (PSA) can be employed to implement an adsorptive capture method on the syngas. These adsorptive systems are particularly suitable for gas flows with lower volumes and higher molar fractions of CO_2, enabling approximately 90% recovery of carbon from the syngas before its combustion as fuel gas [7, 9]. Physical absorption with a liquid solvent is also favored by a high CO_2 partial pressure and it is another great option for pre-combustion separation [87]. If we combine the SCWG plant with a power generation plant, CO_2 can be separated from the flue gases from both the gasifier and the combustion processes [9]. In this case, the common chemical absorption methods with amine-based solvents or pressure vacuum swing adsorption systems (PVSA) are used due to lower partial pressures of CO_2 [9, 88].

An example of a gas-liquid separation system is shown on figure 2.13.

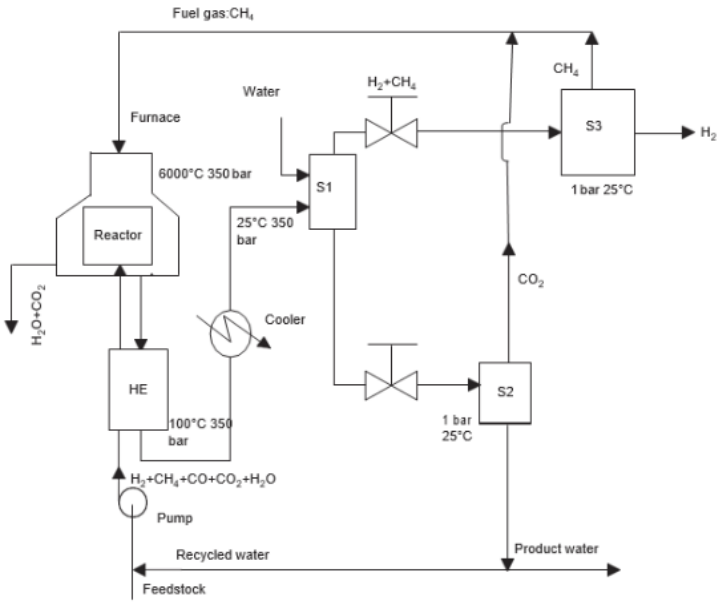

Figure 2.13: Example of a gas-liquid separation system in a SCWG plant [7]

2.7.5 Biomass feed system

Feeding fibrous solid granular biomass into a high-pressure reactor presents significant challenges in the SCWG process. When dealing with a dilute stream of organics, the feeding problem is relatively manageable, as pumps can effectively handle light slurries. However, the situation becomes much more difficult when trying to pump fibrous solid biomass against high pressure. These challenges include [7]:

- Pumping granular biomass: fibrous solid granular biomass, such as agricultural residues or wood chips, can be difficult to pump efficiently against high pressures. The particles in the biomass can clog pumps, leading to decreased efficiency and potential blockages;
- Plugging and deposition: during the pre-heating stage, where the feedstock is heated before entering the gasifier, there's a risk of plugging in the feed lines the feedstock is heated, it can start to break down, forming intermediate products like char. These intermediates can deposit on the walls of the tubing, leading to blockages that hinder the passage of the feedstock. This not only disrupts the process but also poses safety concerns due to potential pressure buildup;
- Equipment wear and maintenance: the abrasive nature of some fibrous biomass materials can cause wear and tear on pumping equipment, leading to increased maintenance requirements and potential downtime.

Proper feedstock preparation, particle size reduction and appropriate feedstock conditioning can help improve pumpability and reduce the risk of blockages. Additionally, the design of the pre-heating stage should take into account potential deposition and plugging issues.

2.8 Combined Heat and Power overview

Combined Heat and Power (CHP) generation presents a sustainable and highly efficient approach to producing electricity using a single fuel source, which can range from natural gas and biomass to coal and oil [89, 90]. This innovative method capitalizes on the surplus heat that is typically wasted in conventional power generation processes. This excess heat, which is generated alongside electricity production, is harnessed and repurposed for various heating applications, such as supplying hot water, space heating, or supporting industrial processes [91]. The core components of most CHP technologies encompass three fundamental elements: the engine or turbine responsible for generating mechanical power, an electrical generator, and heating recovery units, as pointed out in figure 2.14.

A range of CHP systems can be identified, each incorporating different types of engines or turbines. These systems encompass gas turbines,steam turbines, combined steam and gas turbines cycles, organic Rankine cycles, internal combustion engines, Stirling engines and fuel cells [92]. The latter three options in this list are primarily applicable to micro-CHP and small-scale CHP operations, highlighting their suitability for decentralized and localized energy generation scenarios [92].

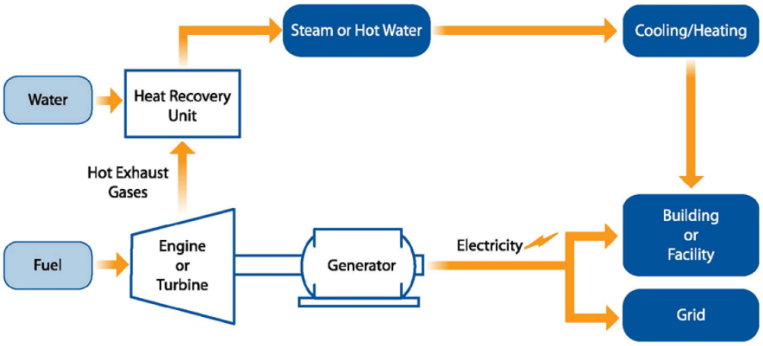

Figure 2.14: Common CHP setup [91]

The thermochemical transformation of biomass and waste materials into energy and fuels while simultaneously generating combined heat and power has emerged as a significant alternative for promoting sustainable development. This approach offers substantial benefits in terms of energy conservation and environmental preservation [93]. Figure 2.15 clearly shows the role of biomass in CHP production on the European Union.

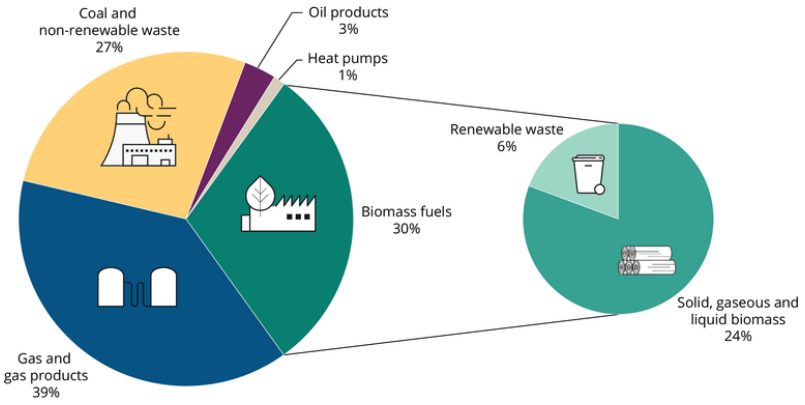

Figure 2.15: EU heat production in CHP and district heating plants, by fuel, in 2020 [94]

Integrating a CHP system demands a thoughtful assessment of various factors including the local energy requirements, the ratio of heat-to-power, the accessibility of fuel resources, and regulatory frameworks [89]. This approach is especially advantageous in scenarios where a consistent and significant need exists for both electrical power and heat. Small and medium-scale CHP setups hold great promise for commercial establishments like hospitals, schools, and office complexes [90]. Additionally, they can serve as effective solutions for decentralized power generation in remote rural regions and on islands [90]. A diagram showcasing the sectors that utilize energy produced from CHP plants in the United States of America (USA) is illustrated in figure 2.16.

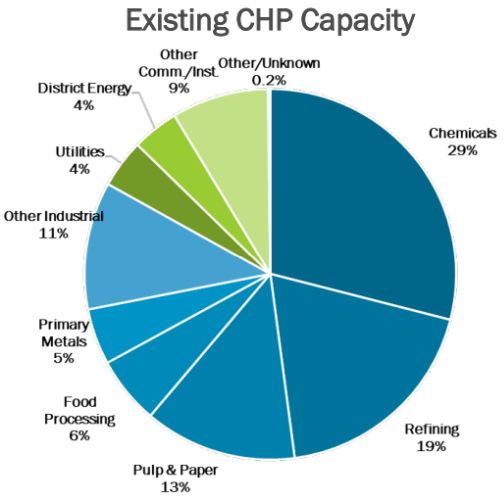

Figure 2.16: CHP capacity distribution by sector in USA as from August 2020 [95]

We can sum up the advantages of CHP systems as [89]:

- Improved Efficiency: some CHP systems can achieve total energy efficiencies of 70% to 90%, whereas conventional power plants typically have efficiencies ranging from 30% to 50%;

- Environmental Impact: CHP systems can help reduce greenhouse gas emissions and lower the overall environmental footprint, as they consume less fuel for the same energy output by being more energy efficient;
- Cost Savings: the use of waste heat for heating purposes can reduce the need for additional heating systems;
- Energy Security: by providing a decentralized and reliable energy source.

2.8.1 CHP production data in the European Union (EU) and Portugal

Collecting and disseminating data from CHP production is of paramount importance for both private and public entities. This practice enables the monitoring of key parameter values over time, facilitates drawing conclusions, and informs decision-making processes. A significant player in this domain is COGEN Europe, the European Association for the Promotion of Cogeneration. According to their mission, they collaborate with EU institutions and stakeholders to shape more favorable policies and remove administrative, regulatory, and market obstacles to the broader adoption of cogeneration in Europe [96]. This association aggregates data from reliable sources such as Eurostat.

In their 2022 COGEN Europe National Snapshot Survey, several graphs were published that unveil significant insights into CHP production. One notable graph, figure 2.17, illustrates the yearly production of heat and power from 2009 to 2019 across the European Union, along with the proportion of electricity production attributed to CHP. Another revealing graph, figure 2.18, presents the same data for Portugal. This specific data was directly sourced from the Eurostat website.

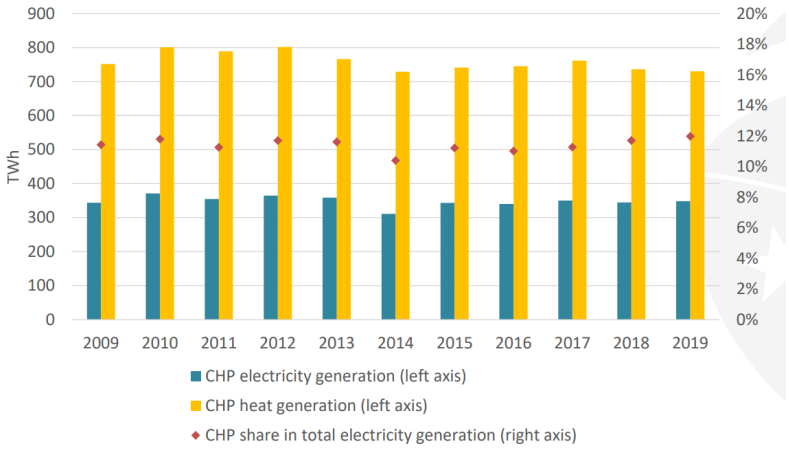

Figure 2.17: CHP production overview on the EU-28 (2009-2019) [97]

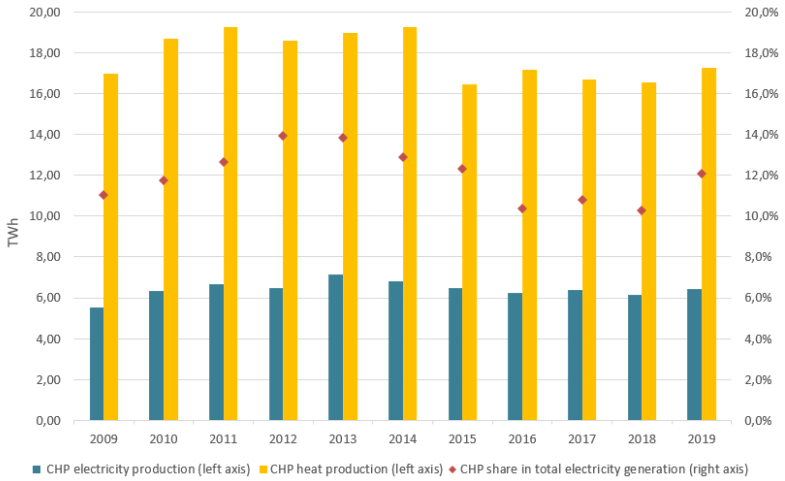

Figure 2.18: CHP production overview on Portugal (2009-2019) [98]

The presented figures highlight that CHP production exhibits oscillations without a discernible consistent trend, a pattern observed in both the EU and Portugal. This phenomenon extends to the share of CHP in gross electricity production. Specifically, the share of electricity generated by CHP plants varies within a range of 12-13% in the EU and 10-14% in Portugal. Notably, the production of heat consistently surpasses that of power, with the heat-to-power ratio being approximately 2.5 to 3 times higher in Portugal and around 2 times higher in the EU.

Continuing in the same COGEN Europe report, an analysis of the fuel mix employed for CHP production in the EU was conducted for the period of 2009 to 2019, as depicted in figure 2.19. Correspondingly, figure 2.20 illustrates the identical data for Portugal, sourced once again from the Eurostat website.

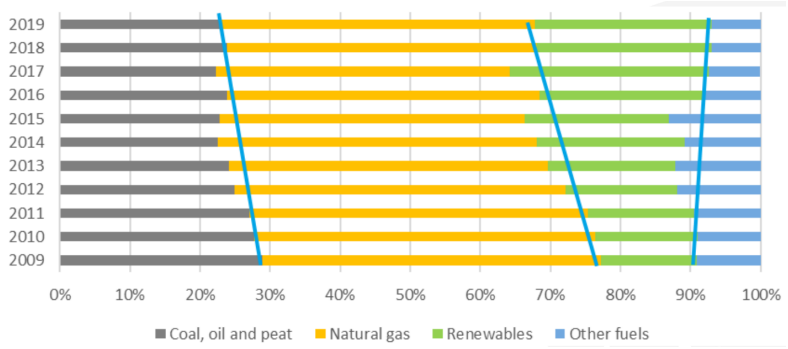

Figure 2.19: EU-28 fuel mix (2009-2019) [97]

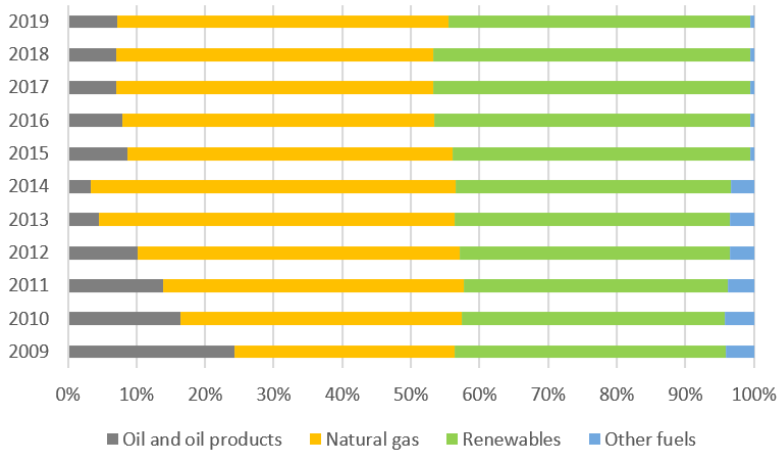

Figure 2.20: Portugal fuel mix (2009-2019) [98]

A noticeable observation from both the EU-28 and Portugal data is that natural gas consumption for CHP production remains robust, constituting approximately 40 to 50% of the fuel mix over the analyzed years. In the context of the EU-28, natural gas stands out without substantial competition, as oil and renewables contribute to a smaller extent (around 20 to 25% of the mix for both sources). Additionally, a discernible pattern emerges with renewables experiencing a modest increase followed by a decrease in oil utilization.

Contrastingly, in Portugal, renewables appear to pose competition to natural gas, especially after an initial decrease in the percentage of oil and other fuels consumption, which in turn has boosted the usage of natural gas.

Shifting focus, another parameter of interest for analysis is the primary energy savings (*PES*) associated with CHP production. *PES* serves as a widely used metric when assessing the environmental impact of a CHP plant. It can be defined as the ratio of energy saved by the CHP system in comparison to an equivalent system with separate gas and steam turbine cycles. This ratio is then divided by the energy consumed in the separated system, as denoted by Eq. 2.17, where F represents the energy content of the utilized fuel and SP pertains to the separated gas and steam turbine cycles [99].

$$PES = \frac{F^{SP} - F}{F^{SP}} = 1 - \frac{F}{F^{SP}} \tag{2.17}$$

Certainly, the limited data availability spanning only three years (2016 to 2018) restricts our ability to draw substantial conclusions from the presented table regarding the evolution of this parameter. Given the short timeframe, a more comprehensive and extended dataset would be necessary to ascertain meaningful trends and patterns in the *PES* metric. It's important to keep in mind that such conclusions often require a longer period to account for potential fluctuations, external factors, and systematic changes that might impact the observed values.

Table 2.4: Energy savings in EU-28 and Portugal in TWh (2016-2018) [98]

	EU-28	**Portugal**
2016	360.15	4.31
2017	374.99	6.53
2018	373.45	5.09

Chapter 3

Modelling and simulation of the SCWG of BSG in Aspen Plus®

Indeed, the complexity of the SCWG process, along with the multitude of variables and parameters that can influence its performance, makes modeling and simulation tools invaluable for understanding, optimizing and predicting its behavior. Instead of relying solely on expensive and time-consuming experimentation, these tools provide a cost-effective and efficient way to explore various scenarios, study the effects of different parameters, and design and optimize SCWG systems [100].

Aspen Plus® is a widely used process simulation software that has proven to be valuable in modeling SCWG processes. It operates based on fundamental principles of mass and energy conservation, as well as chemical equilibrium relations [101]. It allows engineers and researchers to construct detailed process flowsheets, specify reactions, thermodynamic models, and other relevant parameters, and then simulate the behavior of the system under various conditions.

Some benefits of using Aspen Plus® for SCWG modeling include [89]:

- Complex reaction networks: Aspen Plus® can handle complex reaction networks involving multiple chemical reactions, equilibrium constraints and kinetics, which is essential for accurately representing the intricate SCWG reactions;
- Thermodynamic models: the software provides a range of thermodynamic models to accurately describe the behavior of reactants and products under various conditions, accounting for phase changes, heat transfer and more;
- Parametric studies: researchers can conduct parametric studies by systematically varying input parameters to study their effects on the process outcomes, such as gas composition, yields, and energy efficiency;

- Process optimization: Aspen Plus® enables optimization to find the best operating conditions that maximize hydrogen yield, minimize byproducts, or achieve other desired objectives;
- Data visualization: the software generates detailed graphical outputs, allowing users to visualize and analyze the results of their simulations.

3.1 Gasification model

A thermodynamic equilibrium model, often referred to as a zero-dimensional model, is a simplified approach to modeling complex reactions and processes. In the context of SCWG, this type of model assumes that the reacting mixture reaches a state of thermodynamic equilibrium, where the rates of forward and reverse reactions are equal, and no net changes occur in the composition of the mixture over time. This model is particularly useful for studying the influence of various fuel and process parameters on the composition of the final gas without getting into the intricacies of reactor design [7].

The equilibrium model relies on a set of chemical equilibrium equations that describe the distribution of chemical species in the reaction mixture under given conditions of temperature, pressure and feed composition. These equations are based on the principle of minimizing the Gibbs free energy of the system. It's important to note that the thermodynamic equilibrium model provides a simplified representation of the SCWG process, neglecting factors like reaction kinetics, heat and mass transfer limitations and the dynamics of real reactor systems [7]. However, it serves as a valuable tool for gaining insights into how different parameters affect the composition of the gas product and can guide initial process design and optimization efforts. This model assumes [102, 103]:

- Steady state conditions;
- Homogeneous mixing, uniform temperature and pressure;
- Reactions reach the equilibrium state;
- Char is composed only by carbon and its conversion efficiency is 100%;
- Only CO, H_2, CO_2, CH_4 and N_2 compose the final gas;
- Tar formation is not considered;
- Pyrolysis is considered a single step;
- Nitrogen is considered inert;
- Ideal gas behaviour of the gas phase.

The non-stoichiometric approach for this model is based on the minimization of Gibbs free energy and it is a more comprehensive and accurate method for predicting the composition of the final gas in SCWG process, unlike the stoichiometric approach, which relies on predefined reactions and their stoichiometric coefficients [104]. It is particularly well-suited for biomass feedstocks, as their exact chemical composition may not be known precisely [7]. While more computationally intensive, this method provides valuable insights into the thermodynamic behavior of the system and helps optimize process conditions for desired product yields. A set of equations concerning the minimization of the Gibbs free energy are presented as follows [105]. The total Gibbs free energy of the system (G^t) can be defined as:

$$G^t = \sum_{i=1}^{X} n_i \mu_i \tag{3.1}$$

where n_i and μ_i are the number of moles and the chemical potential of specie i, respectively. Assuming an ideal gas behaviour, the chemical potential of specie i can be expressed by:

$$\mu_i = G_i^0 + RTln\left(\frac{f_i}{f_i^0}\right) \tag{3.2}$$

where the R and T represent the universal gas constant and temperature, respectively,f_i is the fugacity of specie i, G_i^0 and f_i^0 denote the standard Gibbs free energy and the standard fugacity of specie i. Fugacity represents a thermodynamic concept indicating a substance's inclination to transition between different environmental compartments [106]. The equation (3.2) can be expressed in terms of pressure as:

$$\mu_i = G_i^0 + RTln\left(\frac{\phi p_i}{p_i^0}\right) \tag{3.3}$$

In the given equation, ϕ represents the fugacity coefficient, which accounts for deviations from ideal behavior in real gases. When the pressure (p) approaches zero, the fugacity coefficient approaches unity ($\phi \rightarrow 1$), and the fugacity (f) approaches the pressure (p). In this context, when the pressure is very low (close to vacuum conditions), the behavior of real gases can be approximated by that of ideal gases. If we assume all gases as ideal gases at a pressure of 1 *atm* we can write:

$$\mu_i = \Delta G_{f,i}^0 + RTln(y_i) \tag{3.4}$$

where y_i is the molar fraction of gas specie i and $\Delta G_{f,i}^0$ expresses the standard Gibbs free energy of formation of specie i that is set to zero for all chemical elements. Introducing equation (3.4) into equation (3.1) it is obtained:

$$G^t = \sum_{i=1}^{X} n_i \Delta G_{f,i}^0 + \sum_{i=1}^{X} n_i RTln(y_i) \tag{3.5}$$

The objective of the problem is to determine the values of n_i which will conduct to the minimization of G^t. The most frequently used method for Gibbs energy minimization is the Lagrange multipliers [107]. The element balance constraint is given by:

$$\sum_{i=1}^{X} a_{ij} n_i = A_j \tag{3.6}$$

where a_{ij} is the number of atoms of the j_{th} element in a mole of i_{th} specie. A_j represents the total number of atoms of the j_{th} element in the reaction mixture. The Lagrangian function (L) is constructed from the total Gibbs free energy (G^t) by considering the mass balances of the system elements [55]. The Langrage multipliers (λ_j=λ_1,...,λ_k) are used by multiplying with elemental balance constraints and those terms are subtracted from G^t obtaining:

$$L = G^t - \sum_{j=1}^{k} \lambda_j \left(\sum_{i=1}^{X} a_{ij} n_i - A_j \right) \tag{3.7}$$

To locate the extremum point, the partial derivatives of equation (3.7) are equated to zero:

$$\frac{\partial L}{\partial n_i} = 0 \tag{3.8}$$

Finally, replacing the value of G^t from equation (3.5) in equation (3.7) and taking its partial derivatives we obtain [103]:

$$\frac{\partial L}{\partial n_i} = \Delta G^0_{f,i} + n_i RT ln(y_i) + \sum_{j=1}^{k} \lambda_j a_{ij} = 0 \tag{3.9}$$

This set of nonlinear equations constitutes n equilibrium equations for every species existing within the system [101]. These equations can be resolved using an iterative approach [105].

3.2 SCWG model

To calculate the properties of biomass and ashes, the HCOALGEN and DCOALIGT models were utilized. The HCOALGEN model, integrated into the Aspen Physical Property System, is particularly designed for estimating enthalpy in scenarios involving coal gasification, particularly for coal with high carbon content but can be applied efficiently for biomass gasification processes. This model accounts for parameters like temperature, pressure, gas composition, and particle size distribution, providing insights into the composition and energy content of the produced syngas, including heat of combustion, heat of formation, and heat capacity [89, 108].

To employ the HCOALGEN model, proximate, ultimate, and sulfur analysis results are required. The sulfur analysis provides weight fractions of sulfur categorized into pyritic, sulfate, and organic sulfur. On the other hand, the DCOALIGT model is suitable for a broader range of coals and encompasses multiple reactions and subprocesses intrinsic to coal gasification, including pyrolysis, tar cracking, char reactions, and gas phase reactions. This model considers various

factors such as temperature, pressure, steam-to-coal ratio, and particle size distribution, necessitating both ultimate and sulfur analysis results. By employing the DCOALIGT model, one can attain more detailed insights into the gasification process, covering aspects like gas composition, tar formation, char conversion, and energy balance [108].

Regarding the properties of conventional components, the RKS-BM method is employed, which stands for the Redlich-Kwong-Soave equation of state with Boston Mathias modifications, in accordance with the software user manual. This method is well-suited for hydrocarbon processing applications and is adaptable to non-polar or lightly polar mixtures over a wide range of temperatures and pressures [109, 110]. It can be represented by the following equation [111]:

$$p = \frac{RT}{V_m - \sum_i y_i b_i} - \frac{\sum_i \sum_j y_i y_j (d_i d_j)^{0.5} (1 - z_{ij})}{V_m (V_m + \sum_i y_i b_i)} \tag{3.10}$$

where V_m is the molar volume, R is the ideal gas constant and T the temperature, d is a parameter calculated by the standard Soave formulation at supercritical temperatures, b is the co-volume parameter, z is a binary parameter determined from phase-equilibrium data regression and y is the molar fraction.

The developed model´s flow diagram is represented in the figure below:

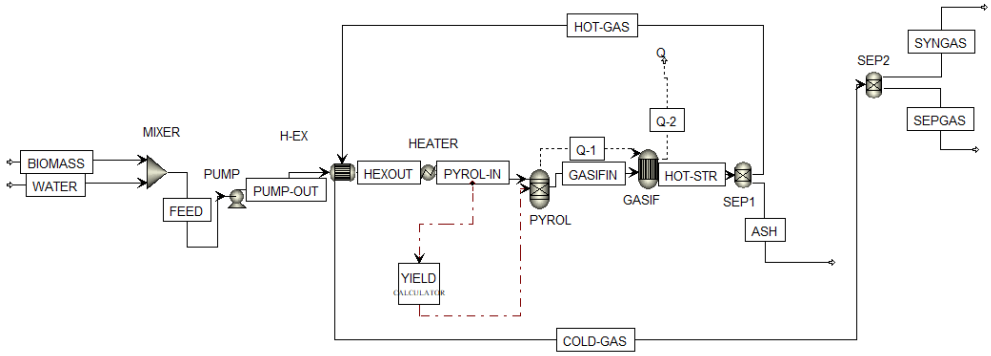

Figure 3.1: SCWG model for hydrogen production in Aspen Plus®

The simulation commences with the combination of water ($WATER$) and the feedstock ($BIOMASS$), identified as a non-conventional component in the software, within a mixer unit ($MIXER$). Mass streams are represented by solid lines, while heat streams are depicted by dashed lines. Following the mixing process, the amalgam of biomass and water undergoes pressurization ($PUMP$) before being subjected to supercritical water conditions through heating. The heating phase unfolds in two stages. Initially, the stream $PUMP-OUT$ is heated utilizing a heat exchanger ($H-EX$) by harnessing the sensible heat from the formed gasification gas ($HOT-GAS$). Subsequently, a second heater ($HEATER$) is employed to reach the designated temperature. Subsequent to this phase, the pyrolysis step follows, responsible for the disintegration of biomass into its core constituents (char, hydrogen, nitrogen, oxygen, sulfur, and ash). This phase transpires in the $PYROL$

unit, designed as a *Ryield* reactor. To oversee the decomposition, a *Fortran* subroutine embedded in the Aspen Plus® scheme, labeled as $YIELD$ calculator, is developed. The distribution of yields is established on the ultimate analysis of the biomass. The heat linked with the pyrolysis process is transferred to the subsequent stage via a heat stream denoted as $Q-1$.

The outcome of the pyrolysis process, designated as $GASIFIN$, proceeds to the $GASIF$ unit where the final step, gasification, takes place. This unit operates as an *RGibbs* reactor, employing the minimization of Gibbs free energy to compute the composition of the resultant gas.

Following the completion of the gasification process, two separations are executed. The first separation is carried out by the $SEP1$ unit, segregating a gas mixture (H_2, CO, CO_2, CH_4, and N_2) from the ash content and residual water. The second separation is facilitated by the $SEP2$ unit, aiming to simulate a carbon capture unit with 100 % capture efficiency. These constituent units comprising the SCWG model function as delineated [112]:

- The *RGibbs* reactor operates on the principles of simultaneous phase and chemical equilibrium modeling. It necessitates specific inputs, namely the reactor temperature and pressure, or alternatively pressure and enthalpy. The reactor leverages the Gibbs free energy minimization approach to facilitate its calculations;
- The *RYield* reactor is employed to determine the yields of individual components within reactions. This reactor proves particularly useful in cases where there is access to yield distribution data or correlations, and when the reaction stoichiometry and kinetics are unspecified;
- The SEP unit serves the purpose of emulating component separation operations based on specific component specifications;
- The $MIXER$ component is capable of determining the combined outlet stream temperature and phase condition using an adiabatic phase equilibrium flash calculation. Its function involves merging various streams (material, heat, or work) into a single outlet stream;
- The $PUMP$ unit changes pressure and is able to calculate the required power given the outlet pressure and vice versa;
- The $HEATER$ can be used to model heaters or coolers with different degrees of subcooling and superheating;
- The $H-EX$ module is equipped to conduct rating calculations for two-stream heat exchangers. It necessitates the specification of both the hot and cold inlet streams, along with either the outlet temperature of the cold or hot stream or the heat exchanger duty.

3.2.1 Model validation

The validation of the SCWG model was done based on the works [113, 114] using glycerol as biomass, with a gasification temperature of 700 and 800$^{\circ}C$, gasification pressure of 241 *bar*

(24.1 *MPa*) and a feed concentration (*f.c.*) of 5 and 20% of biomass. Table 3.1 contains the data regarding the glycerol biomass composition and tables 3.2 to 3.4 contain the obtained syngas composition for the different operating conditions exposed before, ignoring the quantity of N_2. The model can be considered validated as it shows similar hydrogen and carbon dioxide yields to the ones obtained in the literature, showing only considerable errors for the small molar fractions of methane and carbon monoxide.

Table 3.1: Proximate and ultimate analysis of glycerol used on the literature [113, 114]

Proximate analysis *(wt %)*		**Ultimate analysis** *(wt % , daf)*	
Volatile matter	96.17	*O*	52.12
Fixed carbon	2.23	*C*	39.13
Moisture	0.40	*H*	8.70
Ash	1.20	*N*	0.04
		S	0.01

Table 3.2: Relative error between the molar fractions of the syngas produced by the SCWG model in study and the literature studies (*T= 700°C , f.c. = 5%*)

	Model in study	**Experimental study of *Byrd et al* [113]**	**Numerical work of *Hantoko et al* [114]**	**Respective relative errors (%)**	
H_2 (%)	67.30	63.50	66.40	6.00	1.40
CO_2 (%)	32.30	29.10	29.60	11.00	9.10
CO (%)	0.40	0.70	1.40	-45.70	-72.50
CH_4(%)	0.01	6.70	2.70	-99.90	-99.60

Table 3.3: Relative error between the molar fractions of the syngas produced by the SCWG model in study and the literature studies (*T= 800°C , f.c. = 5%*)

	Model in study	**Experimental study of *Byrd et al* [113]**	**Numerical work of *Hantoko et al* [114]**	**Respective relative errors (%)**	
H_2 (%)	69.00	70.00	68.90	-1.50	0.0
CO_2(%)	28.70	25.20	28.60	13.90	0.40
CO (%)	2.00	1.10	2.10	86.40	-2.80
CH_4 (%)	0.30	3.70	0.40	-92.20	-19.40

3.3 BSG used in this study: composition and properties

The BSG biomass used to execute this model simulation is based on the study conducted on [24] regarding steam gasification of a BSG biomass obtained from a Portuguese brewery immediately collected after being separated from the wort.

Table 3.4: Relative error between the molar fractions of the syngas produced by the SCWG model in study and the literature studies (T= *800°C* , *f.c.* = *20%*)

	Model in study	**Experimental study of *Byrd et al* [113]**	**Numerical work of *Hantoko et al* [114]**	**Respective relative errors (%)**	
H_2 (%)	55.70	53.50	55.10	4.10	1.10
CO_2 (%)	28.30	32.90	28.40	-14.00	-0.20
CO (%)	5.50	2.20	5.52	150.00	-0.40
CH_4 (%)	10.40	11.50	11.10	-9.60	-5.90

The chemical composition of BSG in terms of carbon, hydrogen, nitrogen and sulphur were determined using an elemental analyzer and the oxygen percentage by the following difference on a dry and ash-free basis [24]:

$$O(\%) = 100 - C(\%) - H(\%) - N(\%) - S(\%) \tag{3.11}$$

Ash, volatile matter (VM), and moisture (M) contents were measured according to adequate ISO standards and the fixed carbon (FC) by the following equation [115]:

$$FC(\%) = 100 - M(\%) - VM(\%) - Ash(\%) \tag{3.12}$$

The higher heating value (HHV) measured was compared, for its validation, with the correlation found in [116] expressed as:

$$HHV\,(kJ/kg) = 349.1C + 1178.3H + 100.5S - 103.4O - 15.1N - 21.1Ash \tag{3.13}$$

where the mass percentages of the compounds are those obtained by ultimate analysis on a dry basis. The lower heating value (LHV) of the biomass was estimated based on Eq. 3.14 [117]:

$$LHV\,(kJ/kg) = HHV_{biomass} - 2260(0.09H + 0.01M) \tag{3.14}$$

where the value 2260 is the latent heat of steam in kJ/kg. The results obtained after using these equations are presented on table 3.5.

In order to be able to run the simulation an adjustment was needed regarding biomass moisture, decreasing it 0.3% to the value of 78.5% and adding 0.3% to the volatile matter percentage. These values can be checked on table 3.5.

Table 3.5: Proximate and ultimate analysis of the BSG used in this study and its heating values

Ultimate analysis *(wt % , daf)*		**Proximate analysis** *(wt % , d.b.)*		**Heating values** *(MJ/kg)*	
C	48.30	Volatile matter	18.70	*HHV*	17.80
O	38.70	Moisture	78.50	*LHV*	14.89
H	5.60	Fixed carbon	2.0		
N	5.50	Ash	0.80		
S	1.90				

3.4 Parameter variation influence on syngas composition

3.4.1 Effect of varying temperature and pressure of the reaction

As seen on chapter 2.6.1 it is expected an increase of the H_2 molar fraction of the syngas produced together with a reduction of the CH_4 percentage as we increase the reactor temperature. Pressure is expected to have little influence on the composition of the syngas but the study mentioned on chapter 2.6.3 shows that similarly to what happens with temperature we can also favour H_2 production and reduce CH_4 percentages by increasing pressure. To showcase the syngas composition results, a table was made for the pressures of 241, 300 and 350 *bar*, with temperatures ranging from 400°*C* to 1200°*C* to surpass the critical point of water and a graph was plotted to see the evolution of the resultant molar fractions with temperature for a given pressure as shown below:

Table 3.6: Syngas´components molar fractions (%) for different temperatures and pressures

	p= 241 bar				***p= 300 bar***				***p= 350 bar***			
T(°C)	H_2	CO	CO_2	CH_4	H_2	CO	CO_2	CH_4	H_2	CO	CO_2	CH_4
400	30.19	0.03	39.56	26.97	16.85	0.02	42.35	36.90	11.19	0.02	43.54	41.12
500	59.56	0.12	33.36	5.08	55.94	0.12	34.12	7.77	52.54	0.12	34.83	10.31
600	65.99	0.25	31.92	0.26	65.65	0.26	31.98	0.51	65.22	0.27	32.07	0.83
700	66.27	0.38	31.76	0.01	66.26	0.39	31.76	0.02	66.23	0.41	31.75	0.04
800	66.24	0.53	31.66	0.00	66.23	0.54	31.65	0.00	66.23	0.56	31.64	0.00
900	66.18	0.70	31.54	0.00	66.18	0.71	31.53	0.00	66.18	0.73	31.52	0.00
1000	66.12	0.89	31.42	0.00	66.12	0.90	31.41	0.00	66.11	0.91	31.4	0.00
1100	66.06	1.08	31.29	0.00	66.05	1.08	31.28	0.00	66.05	1.09	31.27	0.00
1200	65.99	1.27	31.16	0.00	65.99	1.28	31.15	0.00	65.99	1.28	31.15	0.00

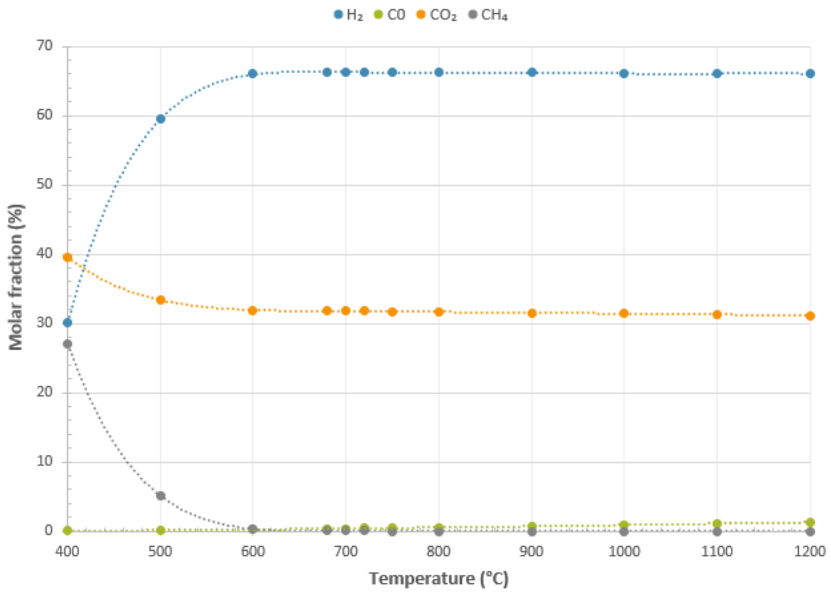

Figure 3.2: Syngas composition variation with temperature for a pressure of 241 *bar*

As expected, a sharp increase in the H_2 molar fraction and a significant decrease of the CH_4 fraction with the rise of temperature can be easily noticed, specially until reaching temperatures around $600°C$. This is due to the methanation reactions (exothermic) being disfavoured with higher temperatures [118]. The CO_2 fraction quantity suffers a small decrease due to the endothermic *Boudouard* reaction [118] and CO increases too little. Surprisingly, a rise on the reactor pressure seems to decrease hydrogen yields, but this is only noticed for low temperature ranges. For higher temperatures hydrogen yields also decrease with a pressure increase, but the variation is too small to take conclusions on the pressure influence. It is to be noted that even though the N_2 data is missing, its molar fraction can be calculated by subtracting the molar fractions of the other components from 100%.

3.4.2 Effect of varying the biomass-to-water ratio (feed composition)

Fixing the temperature and pressure of the reactor as $700°C$ and 241 *bar* respectively, the produced syngas composition was studied varying the feed concentration from 5 to 40% (the lower bound was defined as 5% as this value appears in many papers on SCWG of biomass), obtaining the following results:

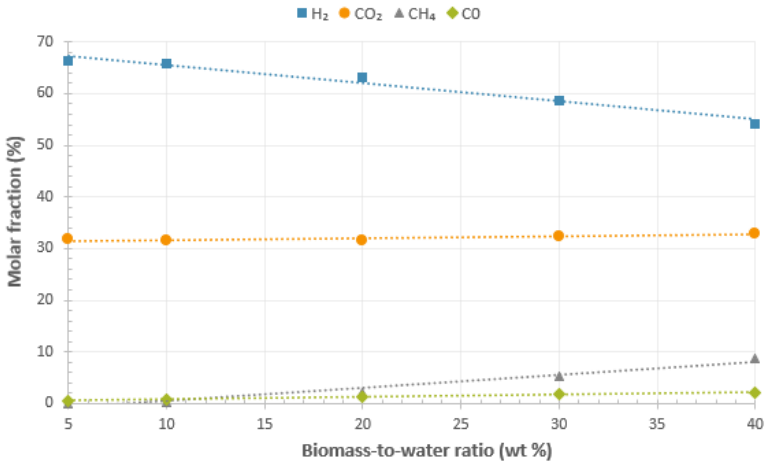

Figure 3.3: Syngas composition variation with feed concentration

As expected from what we have discussed in chapters 2.6.4.1 and 2.6.4.2 a rise in CH_4 molar fraction occurs while a decrease in H_2 is observed with an increase of feed concentration. This occurs because of the inhibition of both the WGS and the steam methane reforming reactions, caused by low water availability. Consequently, the H_2 will react with CO to form CH_4 and CO_2 (dry reforming reaction) [114]. Moreover, the methanation reaction of CO_2 will also take place leading to CH_4 production [119].

3.4.3 Effect of varying the BSG´s moisture percentage

Similarly to what we have seen on the previous chapter,increasing the BSG´s moisture percentage leads to higher hydrogen yields and lower methane yields as it boosts water availability. For the same conditions of temperature and pressure as those in the previous chapter and maintaining the proportion between the other biomass components we obtain the results presented in the following figure:

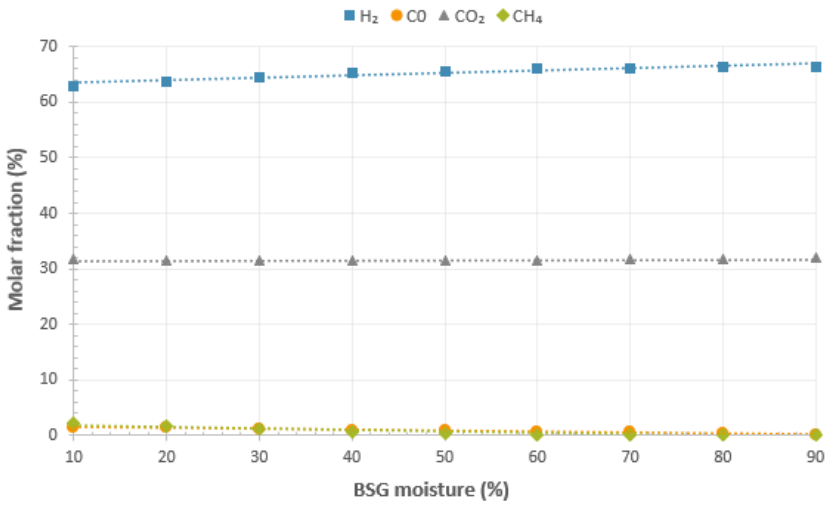

Figure 3.4: Syngas composition variation with feed concentration

From this graph we can conclude, as expected, that the hydrogen fraction increases with the moisture content and the carbon dioxide fraction remains practically constant. On the other hand, the content of carbon monoxide and methane shows a clear decrease even though they show residual percentages as the results are for a quite high gasification temperature ($°C$). This decrease would be more evident if we decrease the operating temperature as CH_4 can show moderate molar fractions. If we increase the moisture content of the BSG up to 100% we obtain ,from our simulation, only hydrogen as a result of water dissociation.

Chapter 4

CHP generation with syngas as fuel: simulation using Aspen Plus®

4.1 CCGT integrated with SCWG power generation: modelling and simulation with Aspen Plus®

The global adoption of biomass gasification for power generation has been steadily increasing. Biomass gasification offers a direct and efficient means of extracting energy from renewable sources and is particularly well-suited for combined heat and power production. The integration of biomass gasification with gas engines for CHP applications presents a significant opportunity for achieving high power efficiency levels, with potential efficiencies reaching up to 40% [120].

Among the various combined cycles, the gas-turbine (Brayton) cycle paired with a steam-turbine (Rankine) cycle has garnered substantial interest due to its superior thermal efficiency compared to the individual cycles. Gas-turbine cycles operate at notably higher temperatures than steam cycles, with modern gas-turbine power plants reaching turbine inlet temperatures exceeding $1425^{\circ}C$, compared to around $620^{\circ}C$ for steam power plants [121]. Advances in turbine blade cooling and the application of high-temperature-resistant materials, such as ceramics, enable the use of these elevated temperatures in gas turbines.

Although gas-turbine cycles hold the promise of achieving higher thermal efficiencies, they also face the challenge of producing high gas temperatures (typically exceeding 500°C) at the turbine outlet, which can negate potential efficiency gains [121]. However, this challenge can be turned to advantage by recovering the energy from the high-temperature exhaust gases and transferring it to steam through a heat exchanger. The steam cycle can further incorporate regeneration and reheating processes, achieved by additional fuel burning, to optimize its efficiency and overall energy recovery [121]. To incorporate a combined cycle that utilizes syngas derived from a SCWG process as its fuel source, we established a connection between our previously developed SCWG model and the combined cycle component of the Aspen Plus® model developed on the paper [90], as illustrated in figure 4.1.

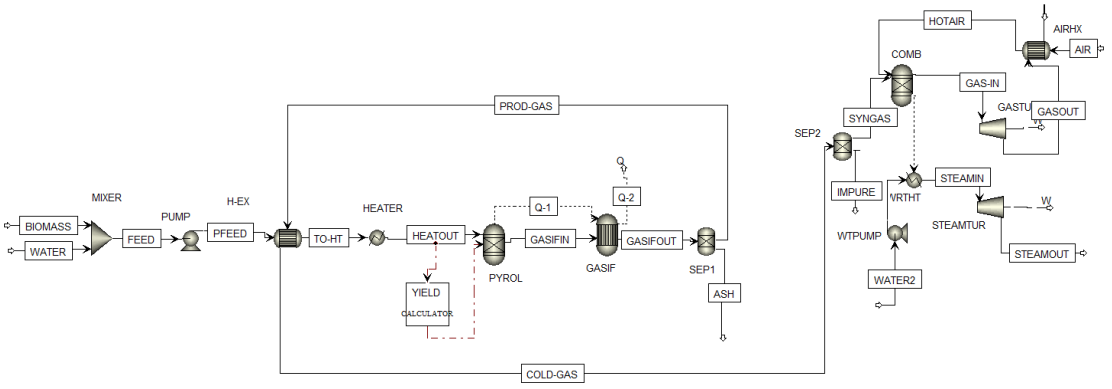

Figure 4.1: Aspen Plus® combined cycle plant integrated with SCWG model

The purified syngas is introduced into a combustion chamber represented by a *RGIBBS* reactor, where it reacts with air, that is heated by the $H-EX$ component ($AIRHX$), to simulate the combustion process. The resulting gases of combustion ($GAS-IN$) are introduced in a gas turbine ($GASTUR$) and the expanded hot outlet gases ($GAS-OUT$) are used to heat this air. Since extremely high temperatures will be achieved during combustion, the excessive heat from this process is used in a $HEATER$ component ($WRTHT$) to produce steam for expansion on the steam turbine $STEAMTUR$, generating additional power. Lastly, the feed water for steam production ($WATER2$) is pressurized on a $PUMP$ module named $WTPUMP$ [90].

4.2 Parameter sensivity analysis and optimization of operating conditions

The main goals of designing a power plant are obviously achieving an efficient way of producing energy, saving both economic and environmental costs. In our case study, as we have a gasification plant that uses the produced syngas as a fuel in a steam and gas turbine combined cycle plant, our goal is to firstly achieve great quantities of good-quality syngas with higher $LHVs$ and that emits less carbon dioxide and other toxic substances to the atmosphere. A good parameter to evaluate the gasification performance on obtaining a good syngas for power generation is the cold gas efficiency ,CGE, that represents the fraction of energy in the biomass feed that can be acquired as energy from the use of the produced syngas and it can be defined as [90]:

$$CGE = \frac{\dot{m}_{syngas} * LHV_{syngas}}{\dot{m}_{BSG} * LHV_{BSG}} \times 100 \tag{4.1}$$

The LHV of the resulting syngas can be determined using the following formula [90]:

$$LHV_{syngas} = \frac{(30X_{CO} + 25.7X_{H_2} + 85.4X_{CH_4}) * 4.2}{1000} MJ/Nm^3 \tag{4.2}$$

where X_{CO}, X_{H_2} and X_{CH_4} are the molar fractions of the species in the syngas, adjusted for the CO_2 removal. As the heating value comes expressed in units of volume, we should replace mass with volume in Eq.4.1.

From this equation we can conclude that the molar fraction of CH_4 has a lot more influence on the LHV value than the other molar fractions. The importance of this and other parameters on the syngas quality is illustrated on table 4.1. As the LHV value is presented per unit of normalized volume, we would have to convert the mass flow of the syngas into a normalized volume flow in order to calculate the cold gas efficiency.

Table 4.1: Desirable syngas characteristics for power production in a turbine [120]

Product/Property	**Requirement**
H_2/CO	Irrelevant
CO_2	Not critical
Hydrocarbons	High
N_2	Irrelevant if burned with a stable flame
Contaminants	Low particulates and metals
Heating value	High
Pressure	about 400 bar
Temperature	500-600$^{\circ}C$

After obtaining the desired syngas the goal is to optimize the steam and gas combined cycle, aiming for a better global efficiency of the system. This can be quantified as the ratio of the net power output, calculated by deducting the auxiliary power consumption from the combined power outputs of the gas and steam turbines, to the energy content present in the BSG biomass, as in the following equation [87]:

$$\eta = \frac{\dot{W}_{GT} + \dot{W}_{ST} - P_{AUX}}{\dot{m} LHV_{BSG}} \times 100 \tag{4.3}$$

Since it is quite hard to calculate with certainty the auxiliary power needed (P_{AUX}) as Aspen Plus® as some limitations regarding power loss calculations (specially for the heat exchangers,heaters and reactors) we will try to find optimum conditions based on our simulation results and considerations from the literature.

For our study we will divide the optimization of the system performance into two steps. Firstly we will study the parameters of gasification that are able to produce a good-quality syngas for its utilization as the fuel for the power production in the designed combined cycle. Since we will simulate an installation with a carbon capture system, the syngas utilized will not have CO_2 and so the power that we can get from its combustion will be given by its LHV and the volume flow of syngas that we obtain after CO_2 removal, parameters that we should optimize.

After having the results for the syngas performance, we will study some parameters that influence the performance of the combined cycle such as gas turbine inlet temperature, air-to-fuel ratio (ratio between the mass flow of air and the mass flow of fuel), air temperature, steam and gas turbine pressure ratios and feed water pressure and flow rate. This way we can understand which syngas can provide the best results for both gas turbine and steam work. Finally, the turbines were assumed to have an isentropic efficiency of 90%.

4.2.1 SCWG optimization for the production of good-quality syngas

To better understand the performance of each syngas when used as a fuel in our combined cycle model we will plot some graphs containing information regarding gas yields and the *LHV* of the syngas (calculated using equation 4.2) to calculate the cold gas efficiency for each case, as it is the parameter that we should optimize to obtain the best power output from the combined cycle. The multiple syngas results were obtained varying gasification temperature, pressure, feed concentration and maintaining the BSG moisture in order to study the performance of a real biomass. For every simulation executed we kept a mass flow of 1000 kg/h of our BSG biomass.

4.2.1.1 Gasification temperature and pressure influence on syngas quality

In this section we will study the influence of gasification temperature and pressure on the produced syngas. Figure 4.2 and figure 4.3 show the *LHV* and syngas volume flow that we can obtain varying the gasification temperature and pressure conditions and fixing 5% of feed concentration. Keep in mind that the high values obtained are due to not counting the CO_2 in molar fraction calculations.

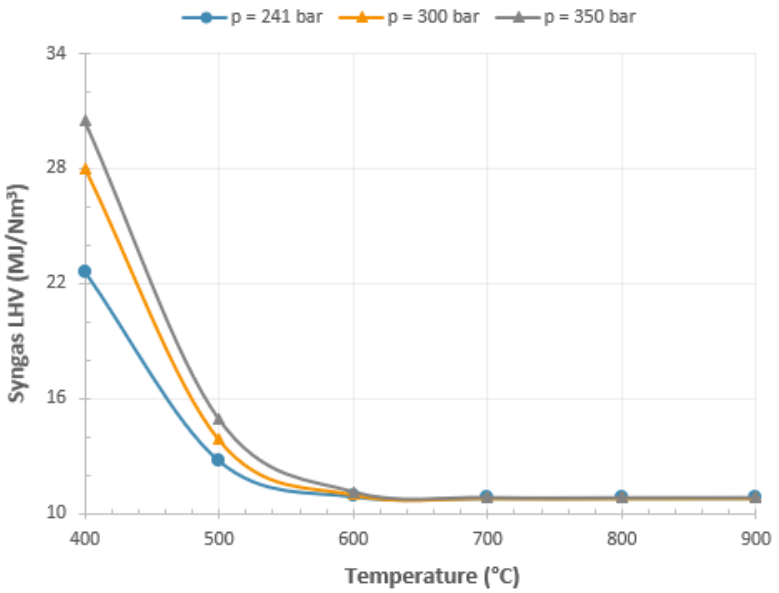

Figure 4.2: Syngas *LHV* results for different gasification pressure and temperature conditions and $f.c. = 5\%$

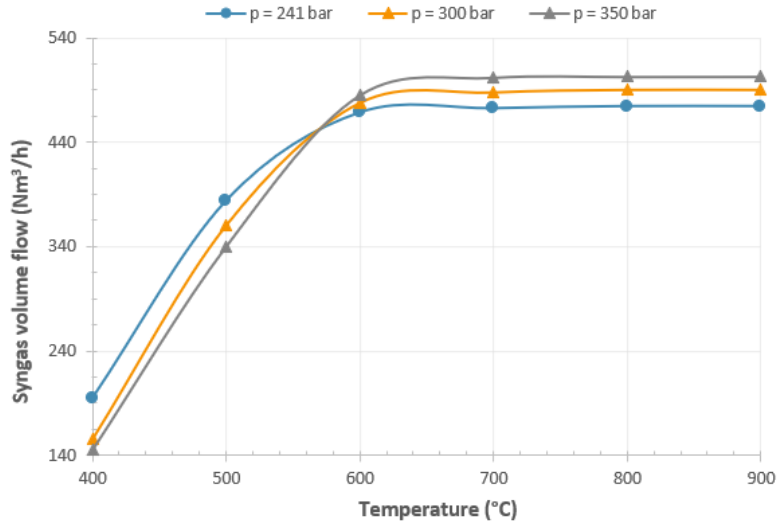

Figure 4.3: Syngas volume flow dependence on temperature , $f.c. = 5\%$

Analysing the first graph (figure 4.2) we come to the conclusion that the *LHV* of the syngas reaches the maximum value at the first temperature considered of $400°C$ decreasing rapidly until reaching $600°C$. After this temperature it quite remains constant and around the *LHV* value for pure hydrogen ($10.8\ MJ/Nm^3$) since we are dealing with syngas with percentages close to 100% hydrogen. The high values for *LHV* at the lowest temperatures can be explained due to the high molar fraction of CH_4 (table 3.6) that strongly enhances the calorific value of the syngas due to its

high coefficient on the *LHV* calculated by equation 4.2. All this happens owing to the methanation reaction being disfavoured with temperature increase and the opposite effect occurs with the WGS reaction, as exposed before on chapter 2.6.1.

In terms of the pressure influence, it seems that it is irrelevant for temperatures above $600°C$ but it increases the *LHV* of the syngas when gasification occurs at lower temperatures since it boosts the CH_4 yields given that CO_2 methanation is a volume decreasing reaction and so higher pressures favours the methanation reaction [122]. Moreover, the values obtained suit the range obtained on the study [24] for the exact same BSG feedstock steam gasification (7.75 to 9.09 MJ/Nm^3) if we calculate the *LHV* for syngas with CO_2.

On the other hand, the volume flow of the syngas shows a completely different evolution while it increases with temperature until reaching the $600°C$ due to the promoted gasification efficiency explained by the greater release of gases during the initial devolatilization phase, as well as the secondary reactions undergone by char and tar (chapter 2.6.1) and also the enhanced supercritical water transport and solvation capacity, explained before on chapter 2.4.1.1 and specially figure 2.6. Note that the volume flow is expressed in normal cubic meters (Nm^3/h) since calorific values of gas fuels are commonly expressed in normalized volume units. In order to convert volume to the normalized one we need to resort to the ideal gas law and write:

$$V_1 = \frac{p_2 T_1 V_2}{p_1 T_2} \tag{4.4}$$

where V_1 is the normalized volume, T_1 = 273.15K, p_1 = 1 atm and the variables with index 2 have the values corresponding to the cold syngas conditions (p_2 = pressure of gasification and T_2 = 323.5K). It is also important to notice that temperatures above $900°C$ are not being considered as they are not viable regarding efficiency and costs but results are available on annex C for a pressure of 241 *bar*. Having the data from these two graphs analyzed, it is easy to plot the cold gas efficiency (CGE):

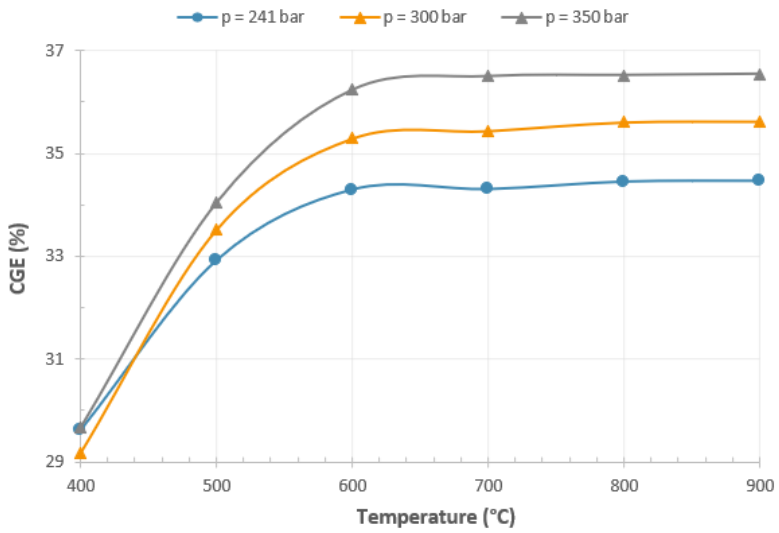

Figure 4.4: Cold gas efficiency evolution with temperature , $f.c.$ = 5%

As expected, CGE increments with temperature and pressure due to the boosted gas yields. Nevertheless, as this parameter is proportional to the product between LHV and syngas volume flow, it was expected that after reaching the temperature of 600°C CGE would remain practically constant. For 600°C it reaches a maximum value of 36.24% while at 900°C scores 36.55%, showing that a further increase in gasification temperature beyond 600°C has no interest due to the economic and energetic cost that comes with it.

Providing that we are studying a system with a carbon capture unit, represented in our model by the unit $SEP2$, it is of paramount importance to see the total CO_2 mass that can be removed after gasification. For that we can check the following graph:

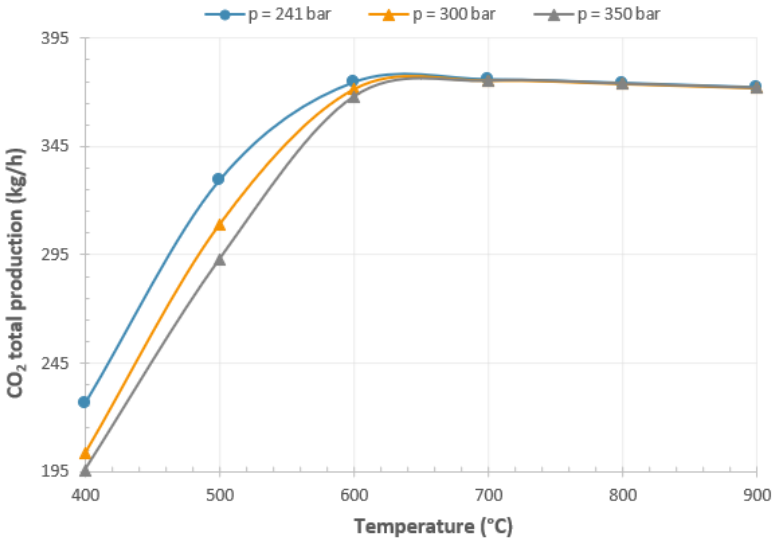

Figure 4.5: Captured CO_2 mass flow for different gasification temperature and pressure conditions, $f.c. = 5\%$

The volume flow of the syngas has a greater influence on the mass quantity of CO_2 produced in comparison with the CO_2 molar fraction, which explains why the graph reaches its maximum value at $600°C$. It is always important to keep in mind that we are assuming 100% efficiency regarding the carbon capture process, in reality these values would differ as this efficiency reduces.

4.2.1.2 Gasification feed concentration on syngas quality

Feed concentration also has an important role on the syngas composition, as seen previously on chapters 2.6.4.2 and 3.4.2. With that being said, we will proceed this work with a similar analysis as the one we just finished doing but varying temperature and feed concentration by adjusting the water content of the feedstock, keeping a pressure equal to 241 *bar*. We will start again by looking at the *LHV* results below:

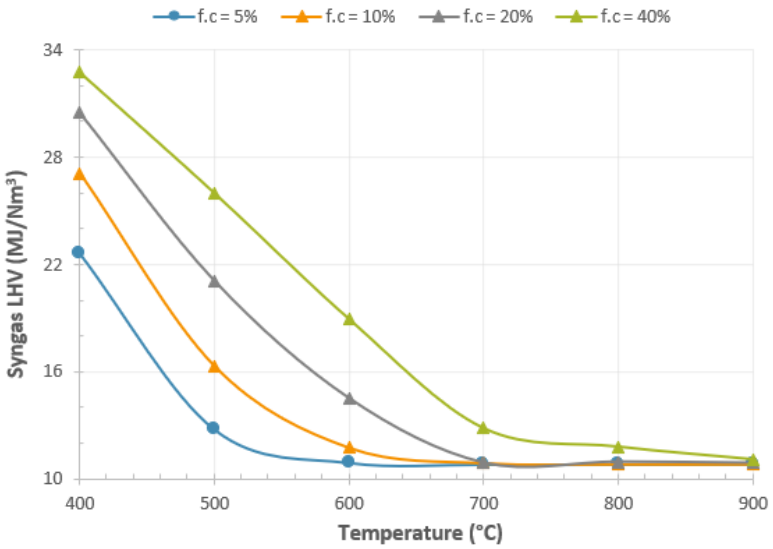

Figure 4.6: Syngas *LHV* results for different gasification temperatures and feed concentrations , p = 241 *bar*

Higher feed concentration means less water if we keep the biomass flow rate constant and equal to the previously defined 1000 kg/h. This way results are comparable, since increasing the biomass percentage would mislead us to higher power values because we are rising our energy source availability.

Higher *LHV* values for also higher feed concentrations happen due to the lower water availability, dropping the hydrogen molar fraction and increasing, on the other hand, the methane molar fraction that has higher influence on the *LHV* estimation (Eq.4.2). Syngas volumes show again an opposite evolution but increasing feed concentration shifts the point were the flow stops to increase significantly to the right on the temperature axis, from 600°C to 700°C for 10% feed concentration, 800°C to 20% feed concentration and to 900°C for 40% feed concentration (figure 4.7), owing to the fact that it is more difficult to achieve high hydrogen yields for feedstocks with less water content, needing higher temperatures for hydrogen generation.

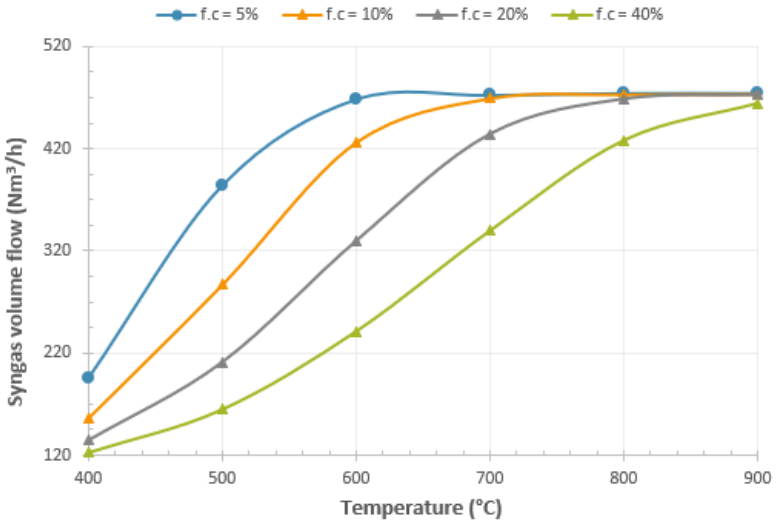

Figure 4.7: Syngas volume flow dependence on temperature and feed concentration , p = 241 *bar*

Before we said that the CO_2 production was more related to the syngas flow than the molar fraction of carbon dioxide itself, this relationship maintains regardless of feed concentration but, as discussed just before, the temperature that achieves maximum volumes shifts to the right with higher feed concentrations, and so does the carbon monoxide production, as we can see in figure 4.8.

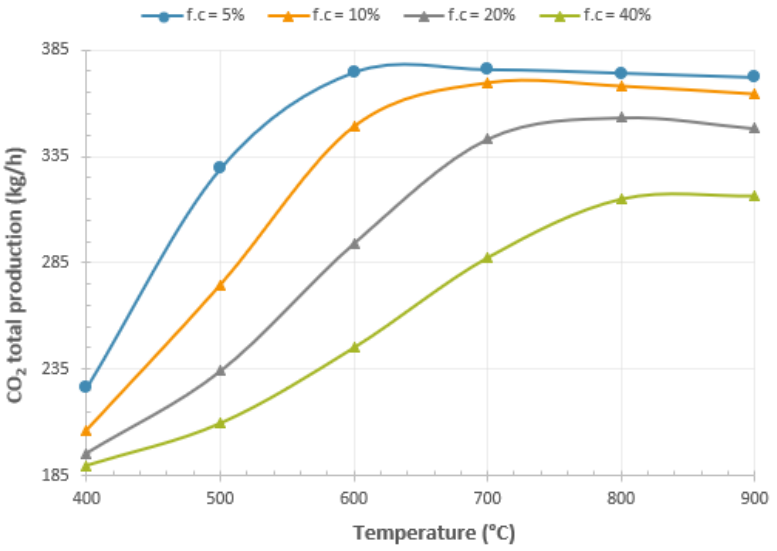

Figure 4.8: Captured CO_2 mass flow for different gasification temperatures and feed concentrations , p = 241 *bar*

Finally, it is no surprise that operating with a feed concentration of 5% shows a clear advantage in comparison to the operation with higher feed concentrations due to the higher syngas volumes,

but this scenario changes from 800°C onwards, temperature where the CGE is basically the same for all three feed concentrations studied. After this point, higher feed concentrations demonstrate higher CGEs. Interestingly enough, for higher feed concentrations there is a noticeable drop on the CGE value around 700°C. This simply happens due to a big reduction of the methane molar fraction, lowering the LHV value, and so the CGE.

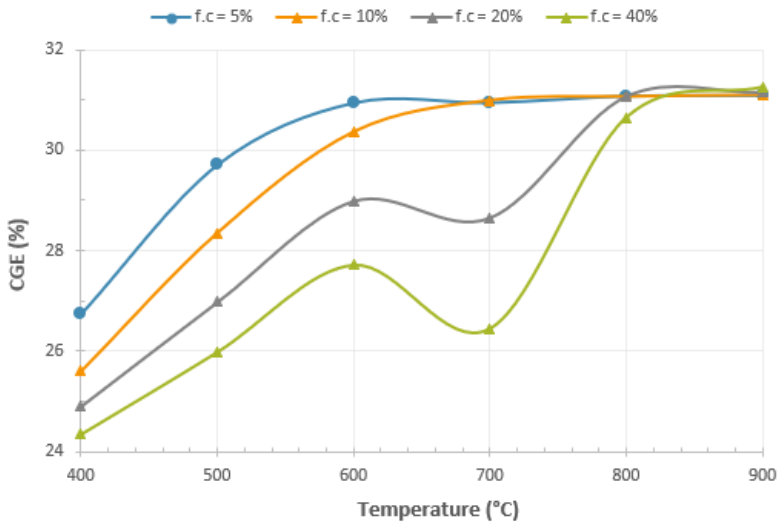

Figure 4.9: CGE evolution with gasification temperature and feed concentrations , p = 241 *bar*

After exposing the results, it becomes necessary to find gasification conditions as close as possible to optimal, that can lead to the production of an efficient and cost effective syngas, with good energy content, to be used in a combined cycle plant.

Operating at a lower pressures and temperatures will lead to huge cost savings as we don´t need incredibly sophisticated equipment that is able to perform under harsh conditions, as well as it will not be needed much additional heat from auxiliary sources. Since there are still a few studies regarding the influence of pressure in SCWG (chapter 2.6.3), we should go for lower pressures such as 241 *bar*.

Observing the lower temperature ranges we can conclude that operating from 400 to 500 °C does not generate a sufficiently efficient syngas and so we should look for higher temperatures. As already seen in our literature review (chapter 2.7.1.2), temperatures higher than 700°C are discouraged if there are no added catalysts to our reactor and so we should look for temperatures ranging from 500 to 700°C.

In this temperature window, 5% and 10% feed concentrations show the best results. However, keeping in mind that we are maintaining the same biomass mass and adjusting water to vary feed concentration, a value of 5% of feed concentrations leads to tremendous costs and pumping efforts since we will have to pressurize a huge amount of water that needs to go through some treatment before it can be pumped to remove turbidity, mainly due to disperse and suspended matter and it

has to be demineralized to prevent the accumulation of minerals in the pipes and devices [123]. Leading with the process effluent with high water content after gas separation also puts us up against some issues and additional costs due to the presence of organic contaminants [124].

With that being said, it seems like a good idea to use a feed concentration around 10% and temperatures between 600 to 700°C as less water would mean saving costs. Since on table 4.1 we are advised to use temperatures from 500 to 600°C for good usage of the syngas on a turbine for power production, we will define our temperature as 600°C.

4.2.2 Combined cycle parameter optimization

Optimizing the combined cycle integrated with the SCWG plant will depend on balancing the work obtained from both turbines since the steam turbine performance highly depends on the gas turbine operating conditions, as it uses steam produced by recovering the excessive heat generated by burning a syngas with high hydrogen yield (with very high adiabatic temperature flames as we will see in chapter 4.2.2.2) in a combustion chamber before the gas turbine expansion occurs. To achieve this, we will study the influence of some parameters like air-to-fuel ratio for syngas combustion, air temperature, combustion temperature, turbine pressure ratios and feed water pressure and mass flow rate.

Before we move on to the parameter analysis of the combined cycle, it is good to show some tables like the ones below, resuming important aspects of our syngas fuel obtained from the SCWG process:

Table 4.2: SCWG parameters to obtain the selected syngas and its properties

BSG mass flow (kg/h)	Feed concentration (%)	Gasification temperature (°C)	Gasification pressure (bar)	Captured CO_2 (kg/h)	CGE (%)
1000	10	600	241	426.23	33.65
H_2 (%)	CO (%)	CH_4 (%)	Volume flow (Nm^3/h)	LHV (MJ/Nm^3)	
95.55	0.67	3.78	348.94	11.75	

4.2.2.1 Air-to-fuel ratio

The first parameter we should analyze is the air-to-fuel ratio (A/F) as it deeply influences the combustion process. We will aim to find the stoichometric value as it is considered the ideal value to have a balance between fuel economy and power. The stoichometric ratio is also used as a base value since it defines the amount of air needed to achieve complete combustion of the fuel. To find this value we can write the combustion equation for our syngas:

- Hydrogen combustion:

$$2H_2 + O_2 \rightarrow 2H_2O \tag{4.5}$$

- Carbon monoxide combustion:

$$CO + \frac{1}{2}O_2 \rightarrow CO_2 \tag{4.6}$$

- Methane combustion:

$$CH_4 + 2O_2 \rightarrow CO_2 + 2H_2O \tag{4.7}$$

Using the molar flows obtained from the simulation model for each component and assuming that the air is composed by 21% O_2 (v/v) we obtain:

$$\dot{n}_{air}(kmol/h) = \frac{\dot{n}_{O_2}}{0.21} = 42.70 \tag{4.8}$$

$$A/F_{st} = \frac{\dot{m}_{air}}{\dot{m}_{syngas}} = 22.13 \tag{4.9}$$

where A/F_{st} is the stoichometric air/fuel ratio.

This high value was expected since our syngas is mainly composed of hydrogen, and the value of A/F_{st} for pure hydrogen is demonstrated to be equal to 34 [125].

4.2.2.2 Air temperature

Not only the A/F plays an important role in the combustion process, air temperature, as shown in table 4.4 can boost the adiabatic flame temperature to a good extent.

Table 4.3: Adiabatic flame temperature for combustion at 1 *bar* and different air temperatures

Air temperature ($^{\circ}C$)	25	40	55	70	100
Adiabatic flame temperature (K)	2400.48	2407.00	2413.50	2419.97	2432.87

With that being said, it is interesting to recover some waste heat of the cycle to heat the inlet air for combustion. In this work, as mentioned in chapter 4.1, we will use the sensible heat from the gases coming from the gas turbine outlet for that purpose. The results are according to the literature since we are obtaining a value of 2400.48 K for the adiabatic flame temperature at ambient conditions for a syngas composed of 95.55% H_2 (table 4.3), close to the 2400 K for pure hydrogen [126].

4.2.2.3 Turbine pressure ratios and feed water variables

When studying a combined cycle our goal is to optimize the performance of the whole cycle and not focus on only one cycle (Brayton cycle for the gas turbine and Rankine cycle for the steam cycle). This is evident as the work output of the steam turbine will depend on the temperature of the steam going through the inlet of the turbine, that depends on the heat provided by the hot gases coming from combustion chamber of the gas turbine. With this configuration, it is expected that the steam turbine will perform better if the temperature of the gas turbine is lower, since

this will lead to more energy recovery from the combustion gases. Nevertheless, it is known from thermodynamics that reducing the inlet temperature of the gas turbine will lead to a smaller efficiency of the process. It is then mandatory to perform an analysis varying all the parameters that can influence the total work output of the cycle and try to arrive to conditions close to optimal.

First we are going to study the influence of the turbine gas inlet temperature and feed water flow rate (wflow) on the total work output of the cycle by analyzing figure 4.10.

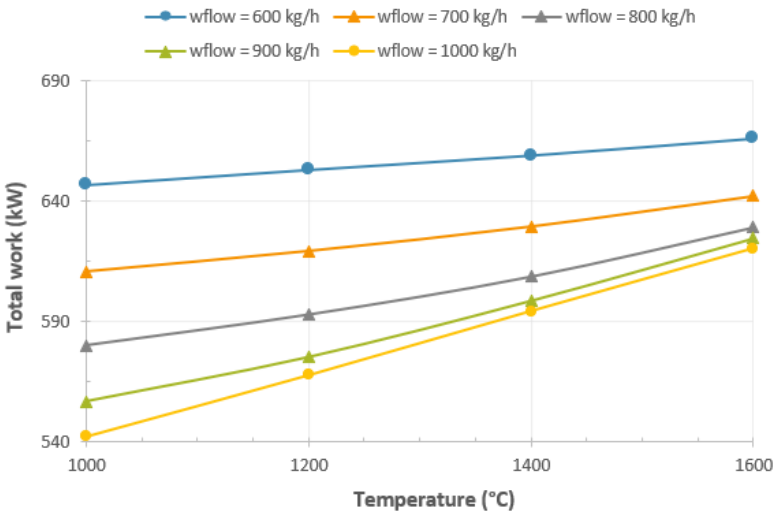

Figure 4.10: Total turbine work for different water feed rates and gas turbine inlet temperatures

In our analysis, a limit of $1600°C$ for the gas turbine operating temperature was set as gas turbines are not able yet to operate much higher than this value. Pressure ratios were fixed to a value that could provide good results. As totally expected, increasing the operating temperature of the gas turbine leads to greater power production as it significantly boosts the gas turbine performance. This can be clarified by observing figure 4.11 related to the steam turbine power generation:

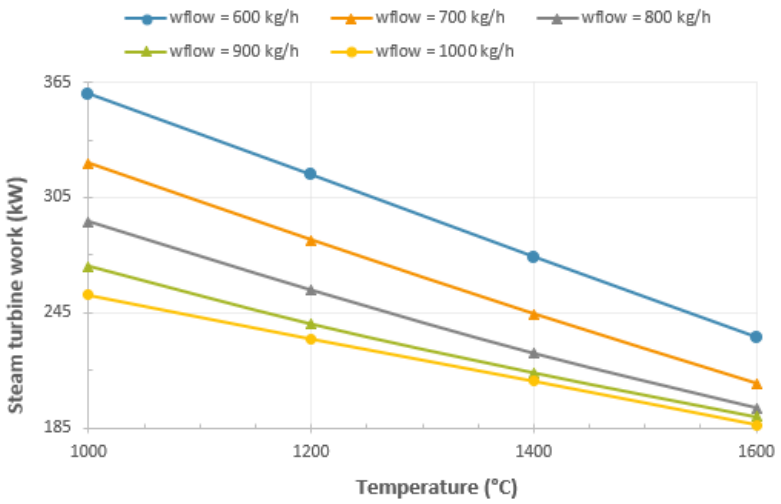

Figure 4.11: Steam turbine output for different water feed rates and gas turbine inlet temperatures

Higher gas turbine temperatures mean that we will have less excess heat available from the hydrogen combustion to spare for steam heating. It is important to insist that this happens in the model we adopted for this work as common combined cycles recover heat from the outlet of the gas turbine. If this was the case the evolution would work the other way.

Talking about feed water flow rate, it becomes clear that an increase in this value reduces the steam work potential due to a reduction in the capacity to heat up the steam leading to lower temperatures at the entrance of the turbine, as shown in the figure below:

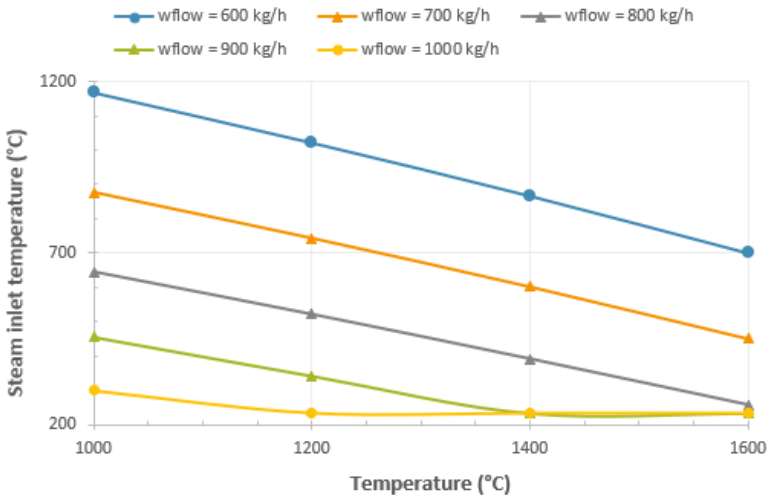

Figure 4.12: Steam inlet temperatures for different water feed rates and gas turbine inlet temperatures

Finally, figure 4.13 shows the influence of both steam turbine and gas turbine pressure ratios

becoming clear that the steam turbine ratio does not influence on the system output. For all the ratios considered it was defined a discharge pressure of 0.1 *bar* since this pressure usually corresponds to the designed pressure of the condenser that can reach 0.03 *bar*. The other way around, pressure ratio is an important parameter when selecting a gas turbine as higher ratios greatly boost system performance.

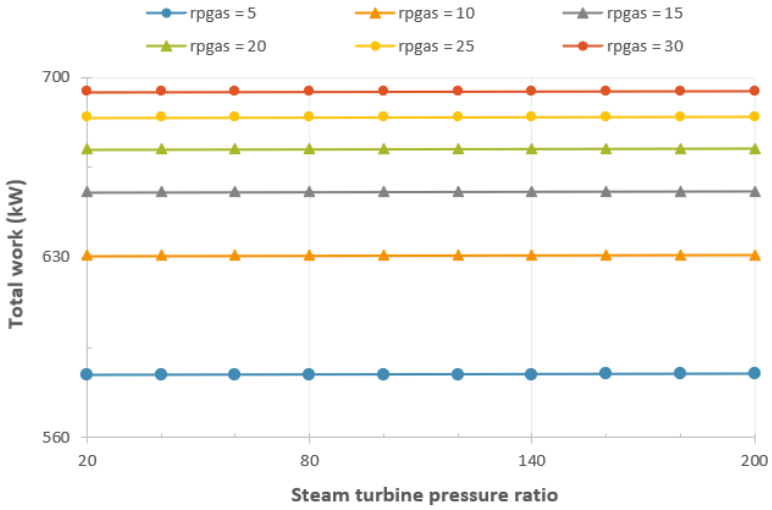

Figure 4.13: Influence of steam and gas turbine pressure ratios on the global work output

4.2.2.4 Defining an optimal point and efficiency estimation

Varying all the discussed parameters except for steam pressure ratio that was fixed in 30*bar* and limiting the steam entrance temperature to around 650°*C* and the gas turbine ratio to 30, as many literature suggests, we obtain the following 8 points corresponding to the cycle operating conditions that produce the greatest amount of work (table 4.4 and 4.5):

Table 4.4: System outputs given by the 4 points corresponding to the highest work output values

Point	Total work (kW)	Gas turbine work (kW)	Steam turbine work (kW)	Steam turbine inlet temperature (°C)	Gas turbine outlet temperature (°C)
1	-686.32	-485.99	-200.32	654.05	721.13
2	-680.85	-485.99	-194.85	597.67	721.13
3	-675.82	-485.99	-189.82	544.27	721.13
4	-671.24	-485.99	-185.24	493.65	721.13
5	-670.82	-468.15	-202.67	633.57	755.61
6	-668.09	-458.34	-209.76	635.03	661.18
7	-667.14	-485.99	-181.14	445.67	721.13
8	-665.5	-468.15	-197.35	579.44	755.61

Table 4.5: Inputs of the 8 points from table 4.4

Point	Gas turbine inlet temperature ($°C$)	Gas turbine pressure ratio	Steam turbine pressure ratio	Feed water flow (kg/h)
1	1600	30	30	580
2	1600	30	30	600
3	1600	30	30	620
4	1600	30	30	640
5	1600	25	30	600
6	1500	30	30	620
7	1600	30	30	660
8	1600	25	30	620

Point 1, corresponding to the point of maximum work obtained for the conditions set, generates 31,4 kg/h of CO_2 from combustion, resulting in an emission factor of 45.75 $kgCO_2/MWh$, emitting 4.4 less carbon dioxide than natural gas, as shown in figure 4.14. However, we ought to consider the amount of 426.23 $kgCO_2/h$ captured before combustion given in table 4.2. This leads to a negative balance of 394.6 $kgCO_2/h$ and a corrected emission factor of -574.95 $kgCO_2/MWh$.

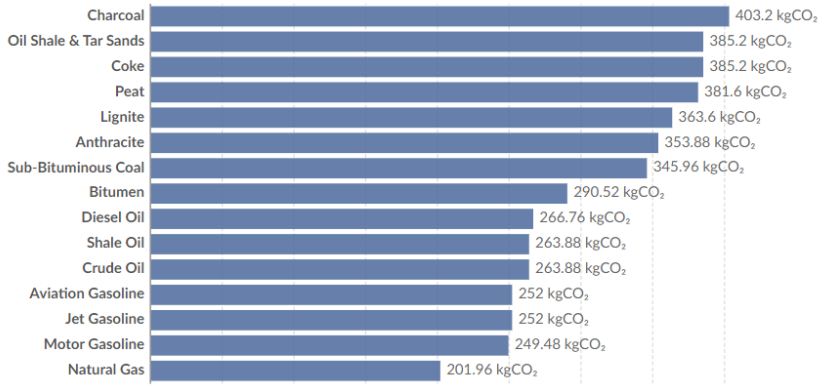

Figure 4.14: Emission factors for different fossil fuels [127]

Finally we can estimate the combined cycle efficiency (η_{CC}) as well as the global plant efficiency (η_G) by writing:

$$\eta_{CC} = \frac{\dot{W}_{total} - P_{losses} - P_{AUX}}{\dot{V}_{syngas} * LHV_{syngas}} \times 100 \tag{4.10}$$

$$\eta_G = CGE * \eta_{CC} \tag{4.11}$$

The plant we have studied is quite complex, being difficult to calculate with certainty the auxiliary energy consumption and the losses, specially for the carbon capture unit that it is not

analyzed with detailed. Equaling these to zero we reach η_{CC} = 49.32% and η_G = 16.6%.

Chapter 5

Conclusions and future works

5.1 Conclusions

Multiple simulations were made to manipulate several parameters that influence the produced syngas compositions and its yields.

It was clearly evident, as the literature states, that an increase in temperature favours the water-gas shift reaction and inhibits the methanation reaction, leading to increased hydrogen yields and total gas yields as well as lower methane yields. In our case, we were able to reach hydrogen molar fractions of around 66% for the syngases produced with only 5% of feed concentration. This happens for lower feed concentratios as water availability is higher. If feed concentration is higher, the production of methane is favoured, reaching 44.75% for a feed concentration of 40%. Pressure also seems to favour the methanation reaction as it states the literature. Keep in mind that all these discussed values can be found in annex *C*.

The calculated *LHV* for each syngas without CO_2 has shown higher values for the lowest temperatures as the methane content was higher, reaching a maximum of 32.75 MJ/Nm^3. It is good to remember that we have obtained such high values due to removing the molar fraction of CO_2 for the calculation, rising the molar fraction values of the other components. With temperature increase, our syngas reaches extremely high molar percentages of H_2 (95-99%) and so the *LHV* converges to that of pure hydrogen (10.8 MJ/Nm^3).

Using the *LHV* values and the volume flows, we calculated the CGE reaching a maximum value of 36.55% for the syngas produced at 900°*C*, pressure of 350 *bar* and 5% feed concentration. This value was quite lower than expected (we could expect values around 60% or even higher) probably due to low gas yields and so we have to clarify what went wrong in a near future.

For the study of the combined cycle performance, we selected the syngas obtained by performing the gasification with a temperature of 600°*C*, pressure of 241 *bar* and 10% feed concentration as it provides a good CGE and the operating conditions of gasification are not that harsh and so more cost-effective.

Concerning the combined cycle, we came to the conclusion that the temperature at the entrance

of the gas turbine and its pressure ratios are the parameters that influence the cycle the most, as well as the air-to-fuel ratio. By limiting the operating temperature of the turbines to feasible values and executing a sensitivity analysis with all the parameters that influence the performance of the cycle, we have reached 686.32 kW of work for the highest gas turbine temperature and pressure ratio defined (600$^{\circ}C$ and 30, respectively), stoichometric air-to-fuel ratio and a BSG feed rate of 1000 kg/h. This lead us to a good effiency of the cycle of 49.32%, but the global efficiency of 16.6% was quite low due to the low CGE. Finally, with this process we can achieve a negative emission factor of 574.95 $kgCO_2/MWh$.

5.2 Future works

First of all, when it comes to the mathematical and thermodynamical aspects of modelling and simulation, it could be intriguing to explore the utilization of kinetic models instead of equilibrium models when studying gasification processes as they are more sophisticated, seeking a deeper understanding of which model type proves to be better suited for simulating biomass gasification. Furthermore, evaluating various Aspen Plus® methods employed for characterizing conventional components' properties, such as the PR (Peng Robinson) and PR-BM (Peng Robinson equation of state with Boston-Mathias function), could also be of great interest.

As seen in chapter 2, there is a paramount interest in exploiting supercritical water gasification with the utilisation of catalysts during the gasification reaction. It would be interesting to add up different catalysts to this model and study the enhancement in system performance that they would provide, specially when it comes to cold gas efficiency. Also, the effect of the size of solid particles in the gasification efficiency could be better explored.

In this work, a carbon capture system was simulated by just adding a separator to the model so that we could use a syngas without carbon dioxide content. For a future work, detailing this carbon capture system would be important since these systems have high costs and their carbon capture efficiency depends on many variables. Analyzing other components´costs would be also interesting.

Finally, other combined cycle models could be tested to improve the efficiency, and also a deeper analysis on the auxiliary consumptions and energy losses should be done in order to provide more accurate results for the efficiency parameters.

References

[1] GES. Yearbook, 2018. Last accessed December 2018.

[2] Jouni Korhonen, Antero Honkasalo, and Jyri Seppälä. Circular economy: the concept and its limitations. *Ecological economics*, 143:37–46, 2018.

[3] PM Townsley. Preparation of commercial products from brewer's waste grain and trub [protein flours]. *Technical Quarterly Master Brewers Association of America*, 1979.

[4] Matthias R Reinold. Manual prático de cervejaria. *São Paulo: Aden*, page 214, 1997.

[5] Solange I Mussatto. Brewer's spent grain: a valuable feedstock for industrial applications. *Journal of the Science of Food and Agriculture*, 94(7):1264–1275, 2014.

[6] Salihu Aliyu and Muntari Bala. Brewer's spent grain: A review of its potentials and applications. *African Journal of Biotechnology*, 10(3):324–331, 2011.

[7] Prabir Basu. *Biomass gasification, pyrolysis and torrefaction: practical design and theory*. Academic press, 2018.

[8] Minh Ho, Guy Allinson, and Dianne Wiley. Reducing the cost of co2 capture from flue gases using pressure swing adsorption. *Industrial Engineering Chemistry Research*, 47, 06 2008.

[9] Gabriel David Oreggioni, Stefano Brandani, Mauro Luberti, Yusuf Baykan, Daniel Friedrich, and Hyungwoong Ahn. Co2 capture from syngas by an adsorption process at a biomass gasification chp plant: Its comparison with amine-based co2 capture. *International Journal of Greenhouse Gas Control*, 35:71–81, 2015.

[10] Kenneth Storm. Chapter 6 - combined cycle power plant (1×1) labor estimate. In Kenneth Storm, editor, *Industrial Construction Estimating Manual*, pages 95–159. Gulf Professional Publishing, 2020.

[11] N.T. Kendal. Barley and malt. In Hardwick W.A., editor, *Handbook of brewing*, pages 109–120. Marcel Dekker.

[12] Kunze Wolfgang. Technology brewing and malting. *YEAST, VLB*, pages 75–83, 1996.

[13] M.J. Lewis and T.W. Young. *Brewing*. Springer US, 2002.

[14] Solange I Mussatto, Giuliano Dragone, and Inês Conceicao Roberto. Brewers' spent grain: generation, characteristics and potential applications. *Journal of cereal science*, 43(1):1–14, 2006.

[15] EGON CARLOS TSCHOPE. Microcervejarias e cervejarias: a história, a arte e a tecnologia. *São Paulo: Aden*, page 223, 2001.

[16] W SCHMIDELL and UA LIMA. Aquarone; e.; borzani, w. *Biotecnologia industrial. Editora*, 2001.

[17] A.M. Macleod. The physiology of malting. In J.R.A. (Ed.) Pollock, editor, *Brewing Science*, volume 1, pages 145–232. Academic Press.

[18] Y Pomeranz and E Dikeman. From barley to beer–a mineral study. *Brewers digest*, 1976.

[19] Nick J Huige. Brewery by-products and effluents. In *Handbook of brewing*, pages 670–729. CRC Press, 2006.

[20] M Santos, JJ Jiménez, Begoña Bartolomé, Carmen Gómez-Cordovés, and MJ Del Nozal. Variability of brewer's spent grain within a brewery. *Food Chemistry*, 80(1):17–21, 2003.

[21] Solange I Mussatto, Marcela Fernandes, and Inês C Roberto. Lignin recovery from brewer's spent grain black liquor. *Carbohydrate Polymers*, 70(2):218–223, 2007.

[22] Nuno GT Meneses, Silvia Martins, José A Teixeira, and Solange I Mussatto. Influence of extraction solvents on the recovery of antioxidant phenolic compounds from brewer's spent grains. *Separation and purification technology*, 108:152–158, 2013.

[23] Solange I Mussatto and Inês C Roberto. Chemical characterization and liberation of pentose sugars from brewer's spent grain. *Journal of Chemical Technology & Biotechnology: International Research in Process, Environmental & Clean Technology*, 81(3):268–274, 2006.

[24] Sérgio Ferreira, Eliseu Monteiro, Paulo Brito, Carlos Castro, Luís Calado, and Cândida Vilarinho. Experimental analysis of brewers' spent grains steam gasification in an allothermal batch reactor. *Energies*, 12(5):912, 2019.

[25] FC Ezeonu and ANC Okaka. Process kinetics and digestion efficiency of anaerobic batch fermentation of brewer's spent grains (bsg). *Process Biochemistry*, 31(1):7–12, 1996.

[26] H Okamoto, Y Kitagawa, T Minowa, and T Ogi. Thermal-catalytic conversion of high moisture spent grains to a gaseous fuel. *Technical quarterly-Master Brewers Association of the Americas*, 36:239–242, 1999.

[27] Mija Sežun, Viktor Grilc, Gregor D Zupančič, and Romana Marinšek-Logar. Anaerobic digestion of brewery spent grain in a semi-continuous bioreactor: inhibition by phenolic degradation products. *Acta Chim Slov*, 58(1):158–166, 2011.

[28] Claire Bougrier, Delphine Dognin, Cécile Laroche, Valérie Gonzalez, Dalel Benali-Raclot, and Jesús Andrés Cacho Rivero. Anaerobic digestion of brewery spent grains: Trace elements addition requirement. *Bioresource technology*, 247:1193–1196, 2018.

[29] Solange I Mussatto, Giuliano Dragone, Pedro MR Guimarães, João Paulo A Silva, Lívia M Carneiro, Inês C Roberto, António Vicente, Lucília Domingues, and José A Teixeira. Technological trends, global market, and challenges of bio-ethanol production. *Biotechnology advances*, 28(6):817–830, 2010.

[30] R Meyer-Pittroff. Utilization of spent brewers' grain for energy production. *Brauwelt*, 128:1156–1158, 1988.

[31] HW Keller-Reinspach. Emissions during the combustion of spent brewer's grains. *Brauwelt*, 129:2316–2319, 1989.

[32] H Okamoto, K Sato, N Yagi, M Inoue, S Yamasaki, S Ishida, and J Shibata. Development of production process of charcoal bricks from spent grain. *Kagaku Kogaku Ronbunshu*, 28(2):137–142, 2002.

[33] K Satoh. Physical property and burning property of spent grain charcoal. *J. Min. Mater.*, 117:587–590, 2001.

[34] André PC Faaij. Bio-energy in europe: changing technology choices. *Energy policy*, 34(3):322–342, 2006.

[35] James G Speight. *Gasification of unconventional feedstocks*. Gulf Professional Publishing, 2014.

[36] Benedetta Ciuffi, David Chiaramonti, Andrea Maria Rizzo, Marco Frediani, and Luca Rosi. A critical review of scwg in the context of available gasification technologies for plastic waste. *Applied Sciences*, 10(18):6307, 2020.

[37] Roger Ruan, Yaning Zhang, Paul Chen, Shiyu Liu, Liangliang Fan, Nan Zhou, Kuan Ding, Peng Peng, Min Addy, Yanling Cheng, et al. Biofuels: introduction. In *Biofuels: Alternative feedstocks and conversion processes for the production of liquid and gaseous biofuels*, pages 3–43. Elsevier, 2019.

[38] Emanuele Graciosa Pereira, Jadir Nogueira Da Silva, Jofran L de Oliveira, and Cássio S Machado. Sustainable energy: a review of gasification technologies. *Renewable and sustainable energy reviews*, 16(7):4753–4762, 2012.

[39] Umberto Arena, Lucio Zaccariello, and Maria Laura Mastellone. Tar removal during the fluidized bed gasification of plastic waste. *Waste Management*, 29(2):783–791, 2009.

[40] Bing-Shun Huang, Hsin-Yi Chen, Kui-Hao Chuang, Ren-Xuan Yang, and Ming-Yen Wey. Hydrogen production by biomass gasification in a fluidized-bed reactor promoted by an fe/cao catalyst. *International Journal of Hydrogen Energy*, 37(8):6511–6518, 2012.

[41] Raghda Ahmed El-Nagar and Alaa Ali Ghanem. *Syngas production, properties, and its importance*, volume 2. IntechOpen London, UK, 2019.

[42] S Amin, RC Reid, and M Modell. Reforming and decomposition of glucose in an aqueous phase. In *Intersociety conference on environmental systems*, number ASME PAPER 75-ENAS-21, 1975.

[43] Yoshikuni Yoshida, Kiyoshi Dowaki, Yukihiko Matsumura, Ryuji Matsuhashi, Dayin Li, Hisashi Ishitani, and Hiroshi Komiyama. Comprehensive comparison of efficiency and co2 emissions between biomass energy conversion technologies—position of supercritical water gasification in biomass technologies. *Biomass and Bioenergy*, 25(3):257–272, 2003.

[44] RAHUL Gupta, AK Mishra, and AK Pathak. Supercritical fluid technology a boon for pharmaceutical particle manufacturing. *Science & Technology For Human Development*, 2014.

[45] A. Malhotra. *Thermodynamic Properties of Supercritical Steam*. Lulu.com, 2009.

[46] Anne Loppinet-Serani, Cyril Aymonier, and François Cansell. Current and foreseeable applications of supercritical water for energy and the environment. *ChemSusChem: Chemistry & Sustainability Energy & Materials*, 1(6):486–503, 2008.

[47] D Lachos-Perez, Juliana M Prado, P Torres-Mayanga, Tânia Forster-Carneiro, M Angela A Meireles, et al. Supercritical water gasification of biomass for hydrogen production: Variable of the process. *Food Public Health*, 5(3):92–101, 2015.

[48] S Heidenreich, M Müller, and PU Foscolo. New and improved gasification concepts. *Advanced Biomass Gasification; Elsevier: Amsterdam, The Netherlands*, pages 98–114, 2016.

[49] Sivamohan N Reddy, Sonil Nanda, Ajay K Dalai, and Janusz A Kozinski. Supercritical water gasification of biomass for hydrogen production. *International Journal of Hydrogen Energy*, 39(13):6912–6926, 2014.

[50] Chai Siah Lee, Alex V Conradie, and Edward Lester. Review of supercritical water gasification with lignocellulosic real biomass as the feedstocks: Process parameters, biomass composition, catalyst development, reactor design and its challenges. *Chemical Engineering Journal*, 415:128837, 2021.

[51] Onursal Yakaboylu, John Harinck, KG Smit, and Wiebren De Jong. Supercritical water gasification of biomass: a literature and technology overview. *Energies*, 8(2):859–894, 2015.

[52] Fiseha Mekonnen Guangul, Shaharin Anwar Sulaiman, and Vijay R Raghavan. Gasification and effect of gasifying temperature on syngas quality and tar generation: A short review. In *AIP Conference Proceedings*, volume 1440, pages 491–498. American Institute of Physics, 2012.

[53] JM Bermudez and B Fidalgo. Production of bio-syngas and bio-hydrogen via gasification. *Handbook of biofuels production*, pages 431–494, 2016.

[54] Ke Qin, Weigang Lin, Peter Arendt Jensen, and Anker Degn Jensen. High-temperature entrained flow gasification of biomass. *Fuel*, 93:589–600, 2012.

[55] In-Gu Lee, Mi-Sun Kim, and Son-Ki Ihm. Gasification of glucose in supercritical water. *Industrial & Engineering Chemistry Research*, 41(5):1182–1188, 2002.

[56] Guanyi Chen, J Andries, Zhongyang Luo, and H Spliethoff. Biomass pyrolysis/gasification for product gas production: the overall investigation of parametric effects. *Energy conversion and management*, 44(11):1875–1884, 2003.

[57] Sonil Nanda, Rachita Rana, Howard N Hunter, Zhen Fang, Ajay K Dalai, and Janusz A Kozinski. Hydrothermal catalytic processing of waste cooking oil for hydrogen-rich syngas production. *Chemical Engineering Science*, 195:935–945, 2019.

[58] Sonil Nanda, Sivamohan N Reddy, Dai-Viet N Vo, Bichitra N Sahoo, and Janusz A Kozinski. Catalytic gasification of wheat straw in hot compressed (subcritical and supercritical) water for hydrogen production. *Energy Science & Engineering*, 6(5):448–459, 2018.

[59] YJ Lu, LJ Guo, CM Ji, XM Zhang, XH Hao, and QH Yan. Hydrogen production by biomass gasification in supercritical water: a parametric study. *International Journal of Hydrogen Energy*, 31(7):822–831, 2006.

[60] Youjun Lu, Liejin Guo, Ximin Zhang, and Chengmeng Ji. Hydrogen production by supercritical water gasification of biomass: explore the way to maximum hydrogen yield and high carbon gasification efficiency. *International Journal of Hydrogen Energy*, 37(4):3177–3185, 2012.

[61] Mitsumasa Osada, Aritomo Yamaguchi, Norihito Hiyoshi, Osamu Sato, and Masayuki Shirai. Gasification of sugarcane bagasse over supported ruthenium catalysts in supercritical water. *Energy & fuels*, 26(6):3179–3186, 2012.

[62] Sonil Nanda, Miao Gong, Howard N Hunter, Ajay K Dalai, Iskender Gökalp, and Janusz A Kozinski. An assessment of pinecone gasification in subcritical, near-critical and supercritical water. *Fuel Processing Technology*, 168:84–96, 2017.

[63] Jude A Okolie, Rachita Rana, Sonil Nanda, Ajay K Dalai, and Janusz A Kozinski. Supercritical water gasification of biomass: a state-of-the-art review of process parameters, reaction mechanisms and catalysis. *Sustainable energy & fuels*, 3(3):578–598, 2019.

[64] W Prins, Sascha RA Kersten, L van de Beld, and JML Penninger. Gasification of wet biomass in supercritical water. In *Handbook Biomass Gasification*, pages 231–247. BTG Biomass technology Group, 2005.

[65] Vichuda Mettanant, Prabir Basu, and James Butler. Agglomeration of biomass fired fluidized bed gasifier and combustor. *The Canadian Journal of Chemical Engineering*, 87(5):656–684, 2009.

[66] H Schmieder, J Abeln, N Boukis, E Dinjus, A Kruse, M Kluth, G Petrich, E Sadri, and M Schacht. Hydrothermal gasification of biomass and organic wastes. *The Journal of Supercritical Fluids*, 17(2):145–153, 2000.

[67] ANDREA Kruse, T Henningsen, A Sınağ, and J Pfeiffer. Biomass gasification in supercritical water: influence of the dry matter content and the formation of phenols. *Industrial & Engineering Chemistry Research*, 42(16):3711–3717, 2003.

[68] Chuang Yang, Shuzhong Wang, Jianqiao Yang, Donghai Xu, Yanhui Li, Jianna Li, and Yishu Zhang. Hydrothermal liquefaction and gasification of biomass and model compounds: a review. *Green Chemistry*, 22(23):8210–8232, 2020.

[69] Adam J Byrd, Sandeep Kumar, Lingzhao Kong, Hema Ramsurn, and Ram B Gupta. Hydrogen production from catalytic gasification of switchgrass biocrude in supercritical water. *International Journal of Hydrogen Energy*, 36(5):3426–3433, 2011.

[70] YJ Lu, Hui Jin, LJ Guo, XM Zhang, CQ Cao, and X Guo. Hydrogen production by biomass gasification in supercritical water with a fluidized bed reactor. *International Journal of Hydrogen Energy*, 33(21):6066–6075, 2008.

[71] Tülay Güngören Madenoğlu, Nikolaos Boukis, Mehmet Sağlam, and Mithat Yüksel. Supercritical water gasification of real biomass feedstocks in continuous flow system. *International journal of hydrogen energy*, 36(22):14408–14415, 2011.

[72] M Mozaffarian, EP Deurwaarder, and S RA Kersten. Green gas (sng) production by supercritical gasification of biomass. 2004.

[73] Daniele Castello, Birgit Rolli, Andrea Kruse, and Luca Fiori. Supercritical water gasification of biomass in a ceramic reactor: Long-time batch experiments. *Energies*, 10(11):1734, 2017.

[74] Ning Ding, Ramin Azargohar, Ajay K Dalai, and Janusz A Kozinski. Catalytic gasification of cellulose and pinewood to h2 in supercritical water. *Fuel*, 118:416–425, 2014.

[75] Demirel Elif and Ayas Nezihe. Hydrogen production by supercritical water gasification of fruit pulp in the presence of ru/c. *international journal of hydrogen energy*, 41(19):8073–8083, 2016.

[76] YH Taufiq-Yap, S Sivasangar, and M Surahim. Catalytic supercritical water gasification of empty palm fruit bunches using zno-doped ni–cao catalyst for hydrogen production. *BioEnergy Research*, 12:1066–1076, 2019.

[77] Ashutosh Kumar and Sivamohan N Reddy. Subcritical and supercritical water in-situ gasification of metal (ni/ru/fe) impregnated banana pseudo-stem for hydrogen rich fuel gas mixture. *International Journal of Hydrogen Energy*, 45(36):18348–18362, 2020.

[78] Kang Kang, Ramin Azargohar, Ajay K Dalai, and Hui Wang. Hydrogen production from lignin, cellulose and waste biomass via supercritical water gasification: Catalyst activity and process optimization study. *Energy Conversion and Management*, 117:528–537, 2016.

[79] Hui Jin, Youjun Lu, Liejin Guo, Ximin Zhang, Aixia Pei, et al. Hydrogen production by supercritical water gasification of biomass with homogeneous and heterogeneous catalyst. *Advances in Condensed Matter Physics*, 2014, 2014.

[80] Tülay Güngören Madenoğlu, Sinem Kurt, Mehmet Sağlam, Mithat Yüksel, Dilek Gökkaya, and Levent Ballice. Hydrogen production from some agricultural residues by catalytic subcritical and supercritical water gasification. *The Journal of Supercritical Fluids*, 67:22–28, 2012.

[81] Tülay Güngören Madenoğlu, Eyüp Yıldırır, Mehmet Sağlam, Mithat Yüksel, and Levent Ballice. Improvement in hydrogen production from hard-shell nut residues by catalytic hydrothermal gasification. *The Journal of Supercritical Fluids*, 95:339–347, 2014.

[82] Jale Yanik, Steve Ebale, Andrea Kruse, Mehmet Saglam, and Mithat Yüksel. Biomass gasification in supercritical water: Ii. effect of catalyst. *International Journal of Hydrogen Energy*, 33(17):4520–4526, 2008.

[83] Obie Farobie, Kazuma Sasanami, and Yukihiko Matsumura. A novel spiral reactor for biodiesel production in supercritical ethanol. *Applied energy*, 147:20–29, 2015.

[84] Edgar Gasafi, Marion-Yvonne Reinecke, Andrea Kruse, and Liselotte Schebek. Economic analysis of sewage sludge gasification in supercritical water for hydrogen production. *Biomass and bioenergy*, 32(12):1085–1096, 2008.

[85] M Riaz, K Barb, and Abraham Engeda. A novel technique for steam turbine exhaust pressure limitation using dynamic pressure sensors. *Proceedings of The Institution of Mechanical Engineers Part C-journal of Mechanical Engineering Science - PROC INST MECH ENG C-J MECH E*, 219:925–932, 04 2005.

[86] Wadim Jäger, Victor Hugo Sánchez Espinoza, and Antonio Hurtado. Review and proposal for heat transfer predictions at supercritical water conditions using existing correlations and experiments. *Nuclear engineering and design*, 241(6):2184–2203, 2011.

[87] C Descamps, Chakib Bouallou, and Mohamed Kanniche. Efficiency of an integrated gasification combined cycle (igcc) power plant including co2 removal. *Energy*, 33(6):874–881, 2008.

[88] Hyungwoong Ahn, Mauro Luberti, Zhengyi Liu, and Stefano Brandani. Process configuration studies of the amine capture process for coal-fired power plants. *International Journal of Greenhouse Gas Control*, 16:29–40, 2013.

[89] OpenAI's ChatGPT. Response to prompt from author. https://chat.openai.com/, 2023. [Online; accessed August 2023].

[90] Th Damartzis, S Michailos, and A Zabaniotou. Energetic assessment of a combined heat and power integrated biomass gasification–internal combustion engine system by using aspen plus®. *Fuel processing technology*, 95:37–44, 2012.

[91] Intergovernmental Panel on Climate Change (IPCC). Carbon dioxide emissions factor. https://ourworldindata.org/grapher/carbon-dioxide-emissions-factor, 2017. [Online; accessed September 2023].

[92] The Renewable Energy Hub. Types of chp and micro chp technology. https://www.renewableenergyhub.co.uk/main/micro-combined-heat-and-power-micro-chp-information/the-different-types-of-chp-and-microchp-technologies, 2023. [Online; accessed August 2023].

[93] M Dentice d'Accadia, M Sasso, S Sibilio, and L Vanoli. Micro-combined heat and power in residential and light commercial applications. *Applied Thermal Engineering*, 23(10):1247–1259, 2003.

[94] European Environment Agency. Gross eu heat production by fuel in chp and district heating plants, 2020. https://www.eea.europa.eu/data-and-maps/figures/gross-eu-heat-production-by, 2023. [Online; accessed August 2023].

[95] U.S. Department of Energy. U.s. department of energy chp installation database. https://chp.ecatalog.ornl.gov/resources/faq, 2020. [Online; accessed August 2023].

[96] COGEN Europe. Who we are. https://www.cogeneurope.eu/about/who-we-are, 2023. [Online; accessed August 2023].

[97] COGEN Europe. 2022 cogen europe national snapshot survey. https://www.cogeneurope.eu/images/COGEN_Europe_Snapshot_Survey_2022_Results_Overview.pdf, 2023. [Online; accessed August 2023].

[98] Eurostat. Chpdata2005-2019.xlsx. https://ec.europa.eu/eurostat/web/energy/database/additional-data#Combined%20heat%20and%20power%20generation%20(CHP), 2023. [Online; accessed August 2023].

[99] Dia Milani. Renewable energy integration in combined cooling, heating, and power (cchp) processes. In *Polygeneration with Polystorage for Chemical and Energy Hubs*, pages 459–491. Elsevier, 2019.

[100] Nuno Couto, Valter Silva, Eliseu Monteiro, PSD Brito, and Abel Rouboa. Modeling of fluidized bed gasification: Assessment of zero-dimensional and cfd approaches. *Journal of Thermal Science*, 24:378–385, 2015.

[101] José Favas, Eliseu Monteiro, and Abel Rouboa. Hydrogen production using plasma gasification with steam injection. *international journal of hydrogen energy*, 42(16):10997–11005, 2017.

[102] María Pilar González-Vázquez, Fernando Rubiera, Covadonga Pevida, Daniel T Pio, and Luís AC Tarelho. Thermodynamic analysis of biomass gasification using aspen plus: Comparison of stoichiometric and non-stoichiometric models. *Energies*, 14(1):189, 2021.

[103] Sérgio Ferreira, Eliseu Monteiro, Paulo Brito, and Cândida Vilarinho. A holistic review on biomass gasification modified equilibrium models. *Energies*, 12(1):160, 2019.

[104] Dipal Baruah and DC Baruah. Modeling of biomass gasification: A review. *Renewable and Sustainable Energy Reviews*, 39:806–815, 2014.

[105] S Jarungthammachote and A Dutta. Equilibrium modeling of gasification: Gibbs free energy minimization approach and its application to spouted bed and spout-fluid bed gasifiers. *Energy Conversion and Management*, 49(6):1345–1356, 2008.

[106] Daniel Vallero. Chapter 5 - life cycle assessment of air pollutants. In Daniel Vallero, editor, *Fundamentals of Air Pollution (Fifth Edition)*, pages 111–133. Academic Press, Boston, fifth edition edition, 2014.

[107] Pertti Koukkari and Risto Pajarre. Introducing mechanistic kinetics to the lagrangian gibbs energy calculation. *Computers & chemical engineering*, 30(6-7):1189–1196, 2006.

[108] Arif Darmawan, Flabianus Hardi, Kunio Yoshikawa, Muhammad Aziz, and Koji Tokimatsu. Enhanced process integration of entrained flow gasification and combined cycle: modeling and simulation using aspen plus. *Energy Procedia*, 105:303–308, 2017.

[109] Peter Akhator and Jude Asibor. Simulation of air-gasification of wood wastes using aspen plus. *International Journal of Engineering Science and Application*, 5(3):86–97, 2021.

[110] Weijuan Lan, Guanyi Chen, Xinli Zhu, Xuetao Wang, Chunmei Liu, and Bin Xu. Biomass gasification-gas turbine combustion for power generation system model based on aspen plus. *Science of the total environment*, 628:1278–1286, 2018.

[111] A. Technology. *Aspen Physical Property System Physical Property Methods and Models*. Cambridge, 2006.

[112] A. Technology. *Aspen Plus ® User Guide*. Cambridge, 2000.

[113] Adam J Byrd, KK Pant, and Ram B Gupta. Hydrogen production from glycerol by reforming in supercritical water over ru/al2o3 catalyst. *Fuel*, 87(13-14):2956–2960, 2008.

[114] Dwi Hantoko, Hongcai Su, Mi Yan, Ekkachai Kanchanatip, Herri Susanto, Guobin Wang, Sicheng Zhang, and Zhang Xu. Thermodynamic study on the integrated supercritical water gasification with reforming process for hydrogen production: Effects of operating parameters. *International Journal of Hydrogen Energy*, 43(37):17620–17632, 2018.

[115] Roberto García, Consuelo Pizarro, Antonio G Lavín, and Julio L Bueno. Biomass proximate analysis using thermogravimetry. *Bioresource technology*, 139:1–4, 2013.

[116] SA Channiwala and PP Parikh. A unified correlation for estimating hhv of solid, liquid and gaseous fuels. *Fuel*, 81(8):1051–1063, 2002.

[117] P Basu and Biomass Gasification. Pyrolysis and torrefaction practical design and theory, 2013.

[118] Deepak Kumar Singh and Jeewan V Tirkey. Modeling and multi-objective optimization of variable air gasification performance parameters using syzygium cumini biomass by integrating aspen plus with response surface methodology (rsm). *International Journal of Hydrogen Energy*, 46(36):18816–18831, 2021.

[119] Sonil Nanda, Sivamohan N Reddy, Howard N Hunter, Ajay K Dalai, and Janusz A Kozinski. Supercritical water gasification of fructose as a model compound for waste fruits and vegetables. *The Journal of Supercritical Fluids*, 104:112–121, 2015.

[120] Eliseu Monteiro and Sérgio Ferreira. Some perspectives for the gasification process in the energy transition world scenario. *Energies*, 16(14):5543, 2023.

[121] Sounak Bhattacharjee. Vapour combined power cycle. http://sounak4u.weebly.com/vapour--combined-power-cycle.html. [Online; accessed August 2023].

[122] Ali Kiani, Lionel Dubois, Remi Chauvy, Renata Lippi, and Rahman Daiyan. Renewable methane production. In *Reference Module in Earth Systems and Environmental Sciences*. Elsevier, 2022.

[123] Ioannis A. Katsoyiannis, Petros Gkotsis, Massimo Castellana, Fabricio Cartechini, and Anastasios I. Zouboulis. Production of demineralized water for use in thermal power stations by advanced treatment of secondary wastewater effluent. *Journal of Environmental Management*, 190:132–139, 2017.

[124] Julian Dutzi, Nikolaos Boukis, and Jörg Sauer. Process effluent recycling in the supercritical water gasification of dry biomass. *Processes*, 11(3):797, Mar 2023.

[125] Ir Ts Dr Mohd Faizal Fauzan. *COMPARITIVE STUDY OF GASOLINE, HYDROGEN AND ALCOHOL FUELED INTERNAL COMBUSTION ENGINES IN TERMS OF SUSTAINABILITY, PERFORMANCE, EMISSION AND ECONOMIC*. PhD thesis, 01 2011.

[126] Zuo-Yu Sun. 11 - hydrogen energy. In Suman Dutta and Chaudhery Mustansar Hussain, editors, *Sustainable Fuel Technologies Handbook*, pages 339–365. Academic Press, 2021.

[127] United States Environmental Protection Agency. What is chp? https://www.epa.gov/chp/what-chp, 2023. [Online; accessed August 2023].

Appendix A

CHP production data

Table A.1: Portugal CHP production data (2015-2019) [98]

Year	CHP power production (TWh)	Share of CHP intotal power generation (%)	CHP heat production (TWh)	Primary energy savings (TWh)
2019	6.43	12.09	17.24	4.62
2018	6.14	10.30	16.55	5.09
2017	6.40	10.80	16.68	6.53
2016	6.25	10.40	17.14	4.31
2015	6.47	12.34	16.47	-

Appendix B

Syngas composition variation with moisture percentage

Table B.1: Syngas composition variation with BSG´s moisture values

	Molar fraction (%)			
BSG moisture (%)	H_2	CO	CO_2	CH_4
10	62.84	1.43	31.69	2.31
20	63.75	1.31	31.59	1.66
30	64.54	1.17	31.53	1.10
40	65.19	1.03	31.50	0.66
50	65.67	0.87	31.52	0.34
60	65.99	0.70	31.58	0.15
70	66.18	0.53	31.67	0.05
80	66.29	0.35	31.78	0.01
90	66.36	0.18	31.90	0.00

Appendix C

Obtained syngas data for different gasification conditions

Table C.1: Data from the syngas obtained with different gasification temperatures for a pressure of 241 *bar* and feed concentration of 5%

T (°C)	H_2 (%)	$C0$ (%)	CO_2 (%)	CH_4 (%)	LHV (MJ/Nm^3)	$\dot{V}$ NO CO_2 (Nm^3/h)	Carbon captured (kg/h)	CGE (%)
400	30.19	0.03	39.56	26.97	22.62	195.02	226.20	29.63
500	59.56	0.12	33.36	5.08	12.76	384.00	329.23	32.92
600	65.99	0.25	31.92	0.26	10.90	468.44	374.56	34.29
700	66.27	0.38	31.76	0.01	10.81	472.46	375.88	34.30
800	66.24	0.53	31.66	0.00	10.81	474.47	374.22	34.45
900	66.18	0.70	31.54	0.00	10.81	474.47	372.22	34.46

Table C.2: Data from the syngas obtained with different gasification temperatures for a pressure of 300 *bar* and feed concentration of 5%

T (°C)	H_2 (%)	$C0$ (%)	CO_2 (%)	CH_4 (%)	LHV (MJ/Nm^3)	$\dot{V}$ NO CO_2 (Nm^3/h)	Carbon captured (kg/h)	CGE (%)
400	16.85	0.02	42.35	36.90	28.00	155.16	203.29	29.19
500	55.94	0.12	34.12	7.77	13.85	360.38	309.05	33.53
600	65.65	0.26	31.98	0.51	10.99	478.01	371.58	35.30
700	66.26	0.39	31.76	0.02	10.81	488.02	375.57	35.44
800	66.23	0.54	31.65	0.00	10.81	490.52	374.04	35.61
900	66.18	0.71	31.53	0.00	10.81	490.52	372.07	35.63

Table C.3: Data from the syngas obtained with different gasification temperatures for a pressure of 350 *bar* and feed concentration of 5%

T (°C)	H_2 (%)	$C0$ (%)	CO_2 (%)	CH_4 (%)	LHV (MJ/Nm^3)	$\dot{V}$ NO CO_2 (Nm^3/h)	Carbon captured (kg/h)	CGE (%)
400	11.19	0.02	43.54	41.12	30.50	144.88	195.66	29.68
500	52.54	0.12	34.83	10.31	14.90	340.11	292.87	34.05
600	65.22	0.27	32.07	0.83	11.12	485.33	367.94	36.24
700	66.23	0.41	31.75	0.04	10.82	502.17	375.26	36.50
800	66.23	0.56	31.64	0.00	10.81	502.99	373.89	36.52
900	66.18	0.73	31.52	0.00	10.81	503.10	371.94	36.55

Table C.4: Data from the syngas obtained with different gasification temperatures for a pressure of 241 *bar* and feed concentration of 10%

T (°C)	H_2 (%)	$C0$ (%)	CO_2 (%)	CH_4 (%)	LHV (MJ/Nm^3)	$\dot{V}$ NO CO_2 (Nm^3/h)	Carbon captured (kg/h)	CGE (%)
400	18.98	0.03	41.91	35.31	27.09	155.93	206.42	28.38
500	48.08	0.16	35.73	13.62	16.32	286.68	274.61	31.43
600	62.93	0.44	32.41	2.49	11.75	426.23	348.94	33.65
700	65.91	0.75	31.56	0.20	10.89	469.58	369.43	34.35
800	66.04	1.06	31.3	0.02	10.83	473.31	367.84	34.43
900	65.95	1.40	31.07	0.00	10.83	473.69	364.12	34.47

Table C.5: Data from the syngas obtained with different gasification temperatures for a pressure of 241 *bar* and feed concentration of 20%

T (°C)	H_2 (%)	$C0$ (%)	CO_2 (%)	CH_4 (%)	LHV (MJ/Nm^3)	$\dot{V}$ NO CO_2 (Nm^3/h)	Carbon captured (kg/h)	CGE (%)
400	11.16	0.03	43.54	41.14	30.51	134.7	195.58	27.60
500	34.21	0.20	38.60	23.94	21.09	211.10	234.12	29.90
600	53.61	0.65	34.20	9.38	14.51	329.72	294.23	32.13
700	65.90	0.75	31.56	0.20	10.89	434.26	343.34	31.76
800	65.37	2.09	30.67	0.26	10.95	468.44	353.38	34.44
900	65.44	2.76	30.15	0.04	10.88	472.46	348.24	34.54

Table C.6: Data from the syngas obtained with different gasification temperatures for a pressure of 241 *bar* and feed concentration of 40%

T (°C)	H_2 (%)	$C0$ (%)	CO_2 (%)	CH_4 (%)	LHV (MJ/Nm^3)	$\dot{V}$ NO CO_2 (Nm^3/h)	Carbon captured (kg/h)	CGE (%)
400	6.31	0.04	44.55	44.75	32.75	122.64	189.76	26.98
500	21.47	0.23	41.23	33.41	26	164.86	209.55	28.80
600	39.87	0.85	36.92	19.55	18.95	241.26	245.06	30.72
700	58.75	1.81	32.26	5.25	12.84	339.77	287.32	29.31
800	61.80	3.80	30.13	2.48	11.81	428.23	314.80	33.97
900	63.99	5.32	28.54	0.48	11.1	464.42	316.27	34.64